

Application of Phytoglycogen in Dry Powder Inhaler Formulation Design

Tse, Jun Yee

Osaka Medical and Pharmaceutical University

Osaka, Japan

2021

Table of contents

Chapter 1 Introduction.....	4
1.1 Pulmonary route as an alternative approach in drug delivery system.....	4
1.2 Trends in preparing DPI formulations	4
1.3 How to define good DPI formulations?	5
1.4 Advantages of spray-drying and importance of excipients in spray-drying.....	7
1.5 Application of macromolecular polysaccharides for DPI formulations.....	10
1.6 Thesis overview	11
Chapter 2 Preparation of novel carrier particle for alveolar delivery	13
2.1 Introduction.....	13
2.2 Results.....	14
2.2.1 Cell viability in lung cells and macrophage-like cell lines	14
2.2.2 Expression of pro-inflammatory cytokine genes	16
2.2.3 Phagocytic activity of macrophage-like cell lines	17
2.2.4 Particle diameter of phytoglycogen	18
2.2.5 Size, loading capacity and percentage yield of spray-dried particles	18
2.2.6 Morphology of spray-dried particles	19
2.2.7 Solid state characterization of particles	20
2.2.8 <i>In vitro</i> aerosolization performance of spray-dried particles	22
2.3 Discussion.....	25
2.3.1 Cell compatibility and the immunostimulatory effect of phytoglycogen.....	25
2.3.2 Effect of solvent composition on phytoglycogen structure.....	26
2.3.3 Formation of porous particles	27
2.3.4 Formation of large-wrinkled particles.....	28
2.3.5 Particle morphology alters deposition behavior.....	30
2.4 Summary.....	32
Chapter 3 Optimization of spray-drying parameters for preparation of formulations with enhanced alveolar delivery	33
3.1 Introduction.....	33
3.2 Results.....	35
3.2.1 Particle morphology of spray-dried particles.....	35
3.2.2 Analysis of the central composite design model.....	36
3.2.3 Influence of inlet temperature, feed flow rate, and gas flow rate on outcomes	48
3.2.4 Optimization of experimental variables – the design space.....	52
3.2.5 Properties of the optimized runs	54
3.3 Discussion.....	58

3.3.1 Behavior of the additives	58
3.3.2 Credibility of the design model.....	59
3.3.3 Relationship between independent and response variables	61
3.3.4 Effectiveness of the design space.....	66
3.4 Summary.....	68
Chapter 4 Conclusions	69
Chapter 5 Experimental section.....	71
5.1 Experimental section of Chapter 2.....	71
5.2 Experimental section of Chapter 3.....	78
Abbreviations.....	82
Acknowledgements.....	83
References.....	84
Published articles	92
Relevant articles.....	92

Chapter 1 Introduction

1.1 Pulmonary route as an alternative approach in drug delivery system

Pulmonary drug delivery formulations are finding broader applications in the pharmaceutical industry with the increased understanding of drug delivery systems^{1,2}. As an alternative method of drug administration targeting the lungs, pulmonary delivery can provide a rapid onset of effect in the lungs and avoid first-pass metabolism, which are attributed to the large surface area of the lungs (40–100 m²), the high permeability of the alveolar epithelial cells, and the low activity of metabolic enzymes^{3,4}. Furthermore, this parenteral administration pathway can generate both local and systemic effects^{5,6}. Recently, nebulizers, metered-dose inhaler, and dry powder inhaler (DPI) formulations have found wide use in treating respiratory diseases. Among these pulmonary dosage forms, DPI formulations are portable, stable, easy to use, and relatively inexpensive. It is also applicable to deliver hydrophobic drugs without propellant gases^{7,8}. For this reason, DPIs have commonly been implemented in treating respiratory diseases like tuberculosis, since some anti-tubercular drugs in the recommended combined treatment have hydrophobic property⁹. Herein, the design, characterization, and optimization of DPI formulation are summarized.

1.2 Trends in preparing DPI formulations

The feasibility of DPI formulations with active pharmaceutical ingredients (APIs) alone depends on their physicochemical properties, in which most APIs are unstable or difficult to inhale. Thus, most of the DPI formulations contain carrier, or so-called excipient additives^{10–12}. The deposition of DPI within the respiratory tract depends on the powder inhalation properties. Lactose is typically included in DPI formulations to improve the powder flow by

providing a coarse carrier for APIs to attach¹³. Nevertheless, coarse carriers may arise issues such as blend uniformity, irritation, coughing, or bronchoconstriction, which diminish the utility of the carrier method. In contrast, bottom-up methods such as spray-drying can employ drugs embedded into a matrix environment provided by excipients, which serves as an alternative strategy for manufacturing composite particles used in DPIs^{14,15}.

1.3 How to define good DPI formulations?

The pharmacological effects of APIs may be enhanced if they are appropriately delivered to the target site. Drug delivery deep into the alveoli is desirable when treating pneumonia, in order to achieve on-target pharmaceutical effects. Thus, the needs of particles with excellent inhalation properties are demanding, as to deliver drugs into peripheral lungs requires technological particle design. One of the most significant parameters to determine the inhalation performance of drugs is the aerodynamic particle diameter, which is calculated by the following equation:

$$\text{Aerodynamic particle diameter } (D_{ae}, \mu\text{m}) = D_{50} \sqrt{\frac{\rho_p}{\rho^*}} \quad \text{Equation 1-1}$$

D_{50} denotes the geometric median particle size, ρ_p represents the particle density, and ρ^* is the unit density (1 g/cm³), which is the reference density for solids. Appropriate control of particle size and morphology can increase the chances of delivering DPI formulations to the anticipated areas of the lungs (**Figure 1-1**).

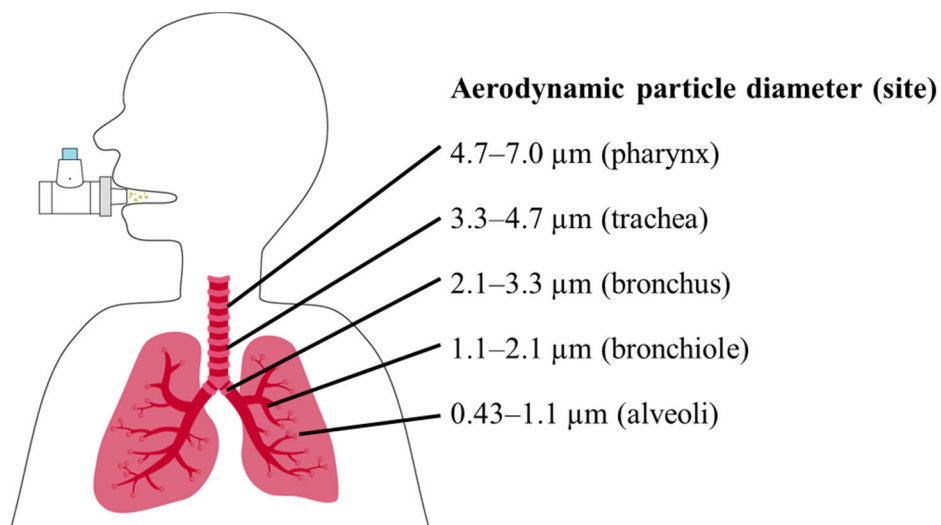


Figure 1-1 Schematic diagram of the relationship between the human respiratory system and particle deposition attributed to aerodynamic diameter

Other than the aerodynamic particle diameter, emitted dose (ED), fine particle fraction (FPF), and extra-fine particle fraction (eFPF) were the inhalation performance metrics. ED represents the proportion of powder that can be released from the capsule and is suppressed by static charges, that trap tiny particles inside the capsule against the inhalation flow¹⁶. FPF is useful for assessing the inhalation properties of general DPI formulations, as it determines the proportion of fine particles with diameters $< 5 \mu\text{m}$ ^{7,17-20}. Among fine particles, extra-fine particles have diameters $< 2 \mu\text{m}$ ^{21,22}; eFPF is the metric used to evaluate the proportion of particles most likely to be delivered to the small airways²¹. Considering the need to control the particle properties, spray-drying is effective to fabricate fine particles, where also has the potential to prepare extra-fine particles.

In terms of productivity and economic feasibility for large-scale production, product yield is also an important indicator of good DPI formulations. To optimize each result including the inhalation parameter such as ED and FPF, Design of experiments (DoE) is a useful tool that statistically links factors and responses, thus can identify important

factors in spray-dried DPI formulations to produce composite particles. Therefore, the application of DoE to the design of DPI formulations can contribute to the development of DPI formulations with ideal inhalation characteristics and productivity based on macromolecular polysaccharide additives.

1.4 Advantages of spray-drying and importance of excipients in spray-drying

The spray-drying method is one of the most popular drying techniques because it is stable, rapid, continuous, cost-effective, and scalable²³. In order to prepare DPI formulations, the spray-drying method has advantages over the traditional coarse carrier method regarding controllable particle properties such as size, shape, and structure²⁴⁻²⁶. Accordingly, this feature is of great advantage to the pulmonary delivery system since the aerodynamic diameter of inhalable particles is critical for determining inhalation performance⁷. Preparation of spray-dried particles (SDPs) containing high dosage of drugs was also reported²⁷⁻²⁹.

The spray-drying method involves atomization, dehydration, and powder collection (**Fig. 1-2**). Dry powders can be recovered from their original precursor by spraying them by an atomizing nozzle into an environment filled with hot gas at a fixed temperature. Although spray-drying is a bottom-up approach that can provide new powder properties to the APIs, the design flexibility is limited unless a proper excipient additive is introduced to the formulation. Excipients can make APIs prominent functions to alter particle morphology, promote stability, and improve solubility. Drug particles are embedded in or attached to the excipient matrix environment by the spray-drying process³⁰. The matrix-structured formulations have attracted a great deal of attention as they aid in overcoming challenges such as poor drug mobility and distribution.

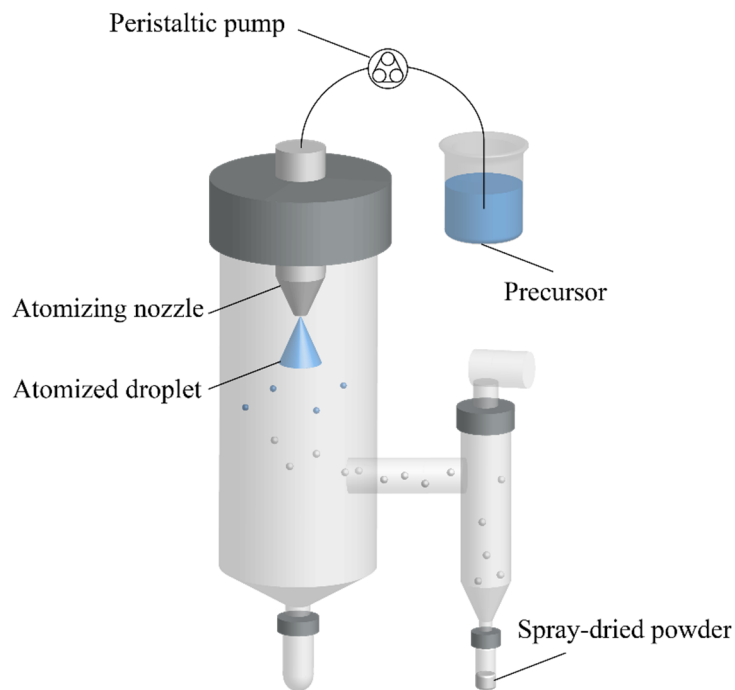


Fig. 1-2 Schematic diagram of spray-drying method

Commonly-used and highly-effective spray-drying additives were limited and listed in **Table 1-1**. Sugars such as lactose and mannitol, synthetic polymers such as poly(lactic-co-glycolic acid), amino acid such as leucine (LEU), and lipid such as dipalmitoylphosphatidylcholine were common additives to be included in the spray-drying precursor. Among the additives, sugars are resource-abundant and have advantages like cheap in cost and have low probability to trigger toxicity in the human body. Their building blocks are usually monosaccharides which have excellent biocompatibility. Although simple sugars like lactose and trehalose were often adopted as DPI carriers, polysaccharides with large molecular sizes have great potential to be adopted as an excipient in DPI formulations within the sugar family.

Table 1-1 List of common or interesting additives for DPI formulations.

Excipient	Example	Characteristics	References
Sugar	Lactose, trehalose	<ul style="list-style-type: none"> ● High hygroscopicity ● Low stability 	31,32
	Mannitol	<ul style="list-style-type: none"> ● Low hygroscopicity ● Crystalline characteristics 	33–35
	Highly-branched cyclic dextrin, phytoglycogen	<ul style="list-style-type: none"> ● Natural polymers with abundant resource ● Ability to form porous particles as a placeholder ● Enhanced drug release 	36,37
Synthetic polymer	Poly(lactic-co-glycolic acid)	<ul style="list-style-type: none"> ● Prolonged drug release ● Low entrapment efficiency 	38,39
Amino acid	Leucine	<ul style="list-style-type: none"> ● Surface modification ● Reduce interparticle forces 	40–42
Lipid	Dipalmitoylphosphatidylcholine	<ul style="list-style-type: none"> ● Major component of pulmonary surfactant ● Surface modification 	43,44

1.5 Application of macromolecular polysaccharides for DPI formulations

The feasibility of using macromolecular polysaccharides as an excipient in DPI has been previously investigated^{45–47}. These studies showed a phenomenon that the particle diameter of the polysaccharides in the solvent increased significantly after the addition of ethanol. The organic solvent acted as a poor solvent to trigger the aggregation of the hydrophilic polysaccharides. As a result, the change of size and morphology of SDP products was observed by altering the precursor composition. This interesting phenomenon also led to an enhancement in the aerodynamic properties, i.e., ED and FPF. Thus, macromolecular polysaccharides have a high potential to act as an excipient for inhalable spray-dried particles. However, the state of drugs varies in a water/ethanol mixed solvent due to their independent properties, a corresponding set of optimized preparation conditions is required for each formulation.

Phytoglycogen (PyG), a macromolecular polysaccharide that is extracted from corn seeds, is known to have a special dendritic structure in an aqueous solution composed of glucose⁵⁰. Same as other sugar additives, PyG is non-toxic, edible, and biodegradable⁴⁸. Other than the dendritic structure, characteristics of a large molecular weight (10^6 – 10^7 Da) and a large median particle diameter in solvents (~50 nm) make PyG prominent to other macromolecular polysaccharides^{49,50}. Despite the potential of PyG to be adopted as an excipient, the properties of PyG-based SDPs had not been discovered. Concerning the foreseeable impact on pulmonary drug delivery, the author aimed attention at the DPI formulation design consisting of a PyG matrix.

1.6 Thesis overview

In Chapter 1, the background and previous studies related to this study are summarized. The purpose and structure of this thesis are also described.

In Chapter 2, the adaptability of PyG as a DPI formulation additive in morphology design was evaluated. Composite SDPs containing rifampicin and PyG were fabricated to characterize the particles in terms of geometric diameter, morphology, and aerosolization performance. The safety of PyG was evaluated by *in vitro* cytotoxicity tests using pulmonary cell lines. The effects of PyG as a functional additive on the expression of pro-inflammatory cytokine genes and phagocytosis in RAW264.7 cells were also investigated.

In Chapter 3, a design of experiments was adopted to optimize the process parameters to prepare DPI formulations with enhanced deep lung delivery ability. The degree of influence of process variables on the properties of the products was also investigated. The performance and validity of the optimization design were evaluated to ensure credibility. Chapters 2 and 3 are outlined in **Fig. 1-3**. The PyG-based DPI formulations were characterized and optimized. Results and knowledge investigated in all chapters served the design of DPI formulation based on PyG.

In Chapter 4, the conclusions of this study are drawn. The contribution made by this thesis was also summarized.

In Chapter 5, the materials and methods used for investigation were described in detail.

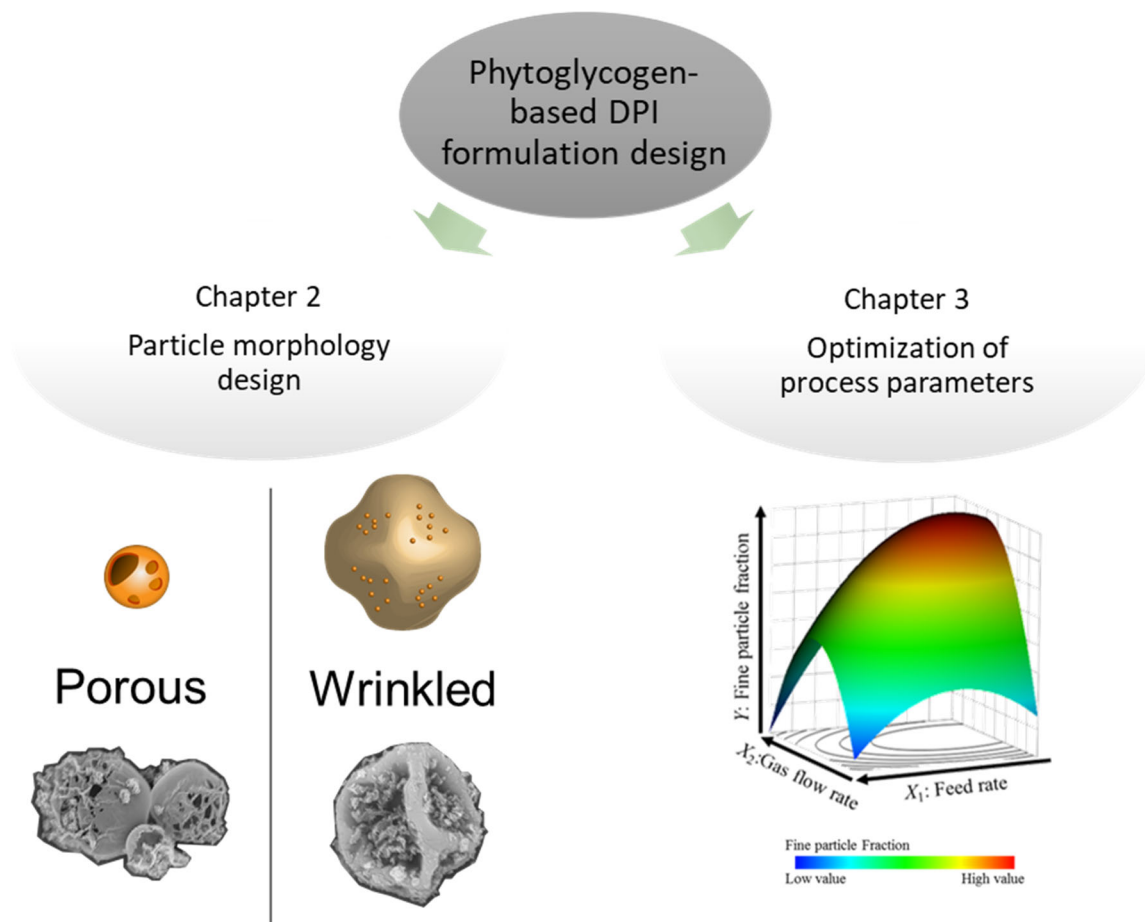


Fig. 1-3 Outline of thesis chapters serving the center idea of phytoglycogen-based DPI formulation design

Chapter 2 Preparation of novel carrier particle for alveolar delivery

2.1 Introduction

The ability of pulmonary formulations to reach the alveolar macrophages is investigated. Taking the antitubercular agent rifampicin (RFP) as an example, the effects on *Mycobacterium tuberculosis* would be robust if the drug could be delivered to the infected alveolar macrophages⁵¹. Inter-particulate agglomeration can hinder the penetration attributed to static charges, even though micronized RFP particles have small aerodynamic diameters¹⁶. Conventional DPI additives such as lactose generally improve the properties of formulations such as uniformity and pulmonary penetration⁵²⁻⁵⁵. The use of small drug particles blended into spherical or coarse granular lactose carriers is a common approach because the use of coarse carriers can effectively decrease the agglomeration rate of micronized drug particles^{3,13,56}. As a disadvantage, the lactose particles often do not pass the throat during inhalation because of their size, leading to side effects such as coughing and bronchoconstriction. Moreover, the uniformity issue is an obstacle for carrier-based pulmonary formulations. To tackle the challenges, scientists prepared low-density porous particles that were favorable for inhalation because of their small aerodynamic particle diameter^{24,53,57-60}. On the other hand, wrinkled particles may also entrap smaller detachable particles for advanced penetration³⁵. Among the precursor properties, solvent composition, surface tension, and viscosity may be determining factors owing to their influence on the droplet drying rate and shell formation^{61,62}. The surface tension and viscosity are the main influences on the drying mechanics of atomized droplets⁶³⁻⁶⁵. In this chapter, the morphology of drug-containing SDPs is manipulated by adjusting the solvent composition of the precursor. Porous and large-wrinkled particles were prepared by different

approaches. The differences in formation mechanism and alveolar delivery rate between these two morphologies are of interest for designing inhalable formulations using the macromolecular polysaccharide PyG.

An *in vitro* cytotoxicity test using lung cell lines is a basic and effective evaluation. To further verify the potential of PyG as an inhalable excipient, the cytotoxicity was tested in A549 and Calu-3 lung cells and RAW264.7 macrophage-like cells. The effects of PyG on the expression of pro-inflammatory cytokine genes and phagocytosis in RAW264.7 cells were also investigated. To further characterize the particles in terms of geometric diameter, morphology, and aerosolization performance, SDPs of PyG only and composite SDPs containing RFP and PyG were fabricated.

2.2 Results

2.2.1 Cell viability in lung cells and macrophage-like cell lines

The WST-8 assays were carried out to determine the cytotoxic effects of PyG on A549 and Calu-3, and RAW264.7 cells. No apparent cytotoxic effect was detected up to a concentration of 1 mg/mL of PyG on A549, Calu-3, and RAW264.7 cells, as no significant differences were found between the groups (**Figs. 2-1&2**). These results suggest that PyG can be safely used as a DPI additive.

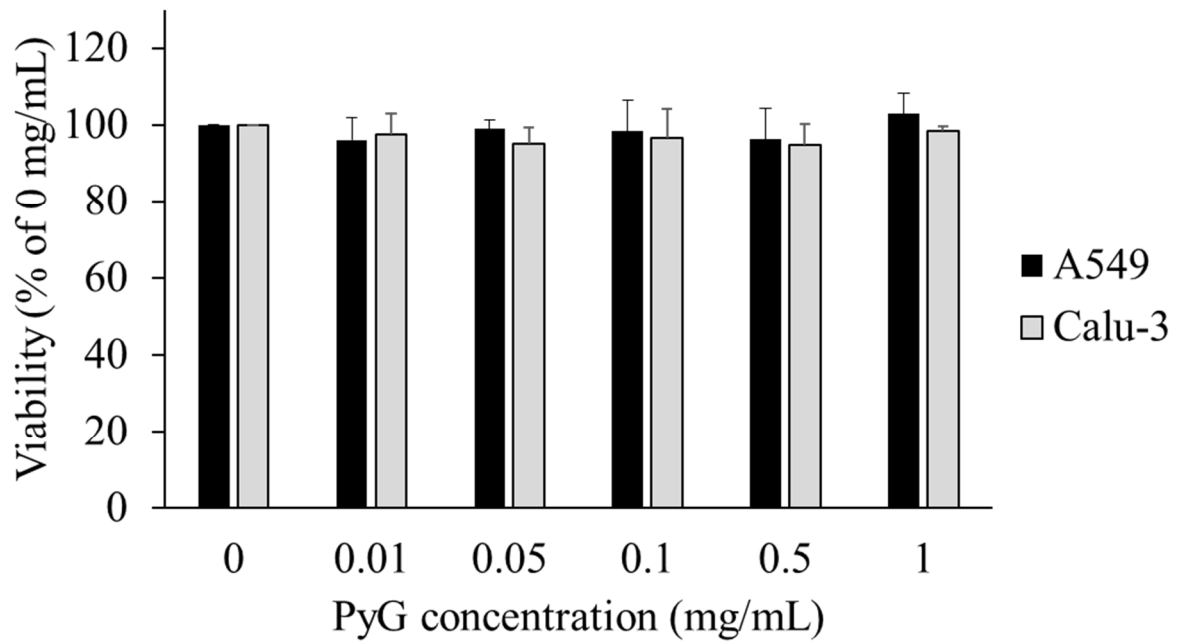


Fig. 2-1 Cell viability of A549 and Calu-3 cells exposed to phytyglycogen for 24 h, evaluated using a Cell Counting Kit-8. Values are represented as mean \pm standard deviation (SD, n = 3)

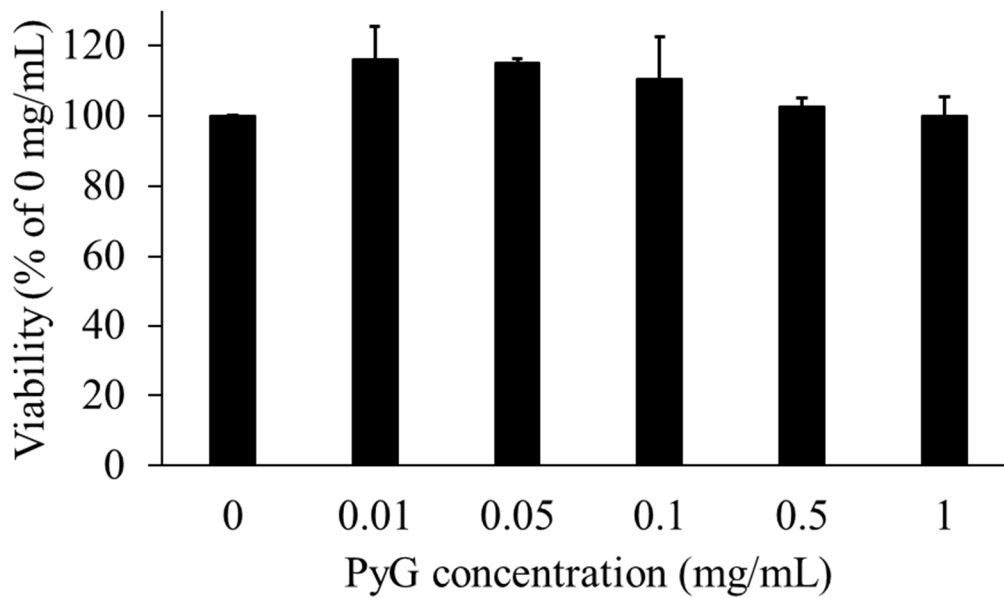


Fig. 2-2 Cell viability of RAW264.7 cells exposed to phytyglycogen for 24 h, evaluated using a Cell Counting Kit-8. Values are represented as mean \pm SD (n = 3).

2.2.2 Expression of pro-inflammatory cytokine genes

The expression of pro-inflammatory cytokine genes in PyG-treated RAW264.7 cells was determined by quantitative PCR (Fig. 2-3). The gene expression of IL-1 β , iNOS, and TNF- α was analyzed after treatment with various concentrations of PyG for 24 h. When the cells were incubated with 0.01–0.2 mg/mL of PyG, the expression level of the IL-1 β , iNOS, and TNF- α genes was low, which was almost the same level as 0 mg/mL, except for TNF- α level at 0.1 mg/mL. Whereas, when the cells were treated with PyG at 0.5–1 mg/mL, the expression level of these genes significantly increased. These results indicate that PyG has the potential to exert an immunostimulatory effect as a DPI additive.

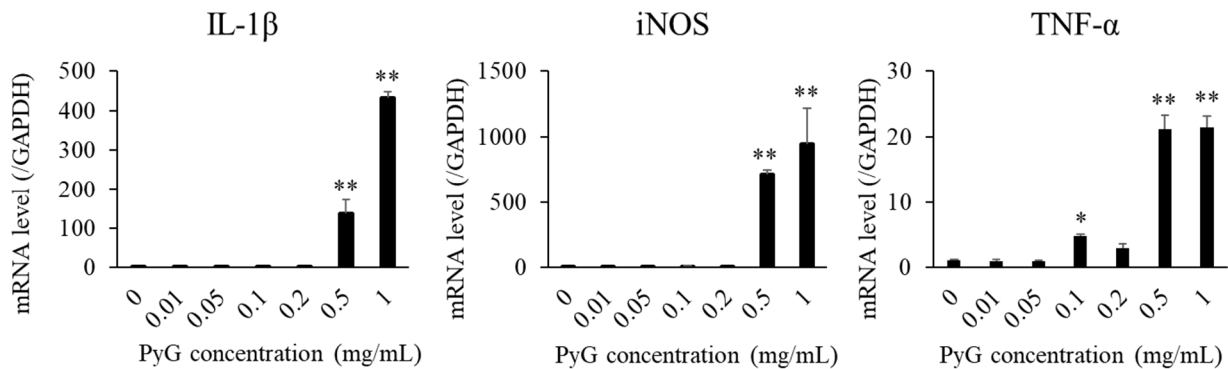


Fig. 2-3 Expression of pro-inflammatory cytokine genes: IL-1 β , iNOS, and TNF- α in phyto glycogen-treated RAW264.7 cells. Values are represented as mean \pm SD (n = 3). (* p < 0.05, ** p < 0.01, vs. 0 mg/mL)

2.2.3 Phagocytic activity of macrophage-like cell lines

The effect of PyG on the uptake of latex beads by RAW264.7 cells was investigated (**Fig. 2-4**). When RAW264.7 cells were treated with high PyG concentrations (0.5–1 mg/mL), the fluorescence intensities were higher than those in the cells treated with low PyG concentrations (0–0.01 mg/mL) (**Fig. 2-4a**). Next, the intracellular fluorescence derived from the polystyrene latex beads and Hoechst 33342 is measured. The quotient of fluorescence of latex beads and Hoechst was plotted against the PyG concentration. When the cells were treated with high concentrations of PyG (0.5–1 mg/mL), the cellular uptake of latex beads was approximately two-fold higher than those with low concentrations of PyG (0–0.01 mg/mL) (**Fig. 2-4b**). In addition to the increased expression of pro-inflammatory cytokine genes, the increase in cellular uptake further shows the potential immunostimulatory effect of PyG, which results in increased phagocytic activity.

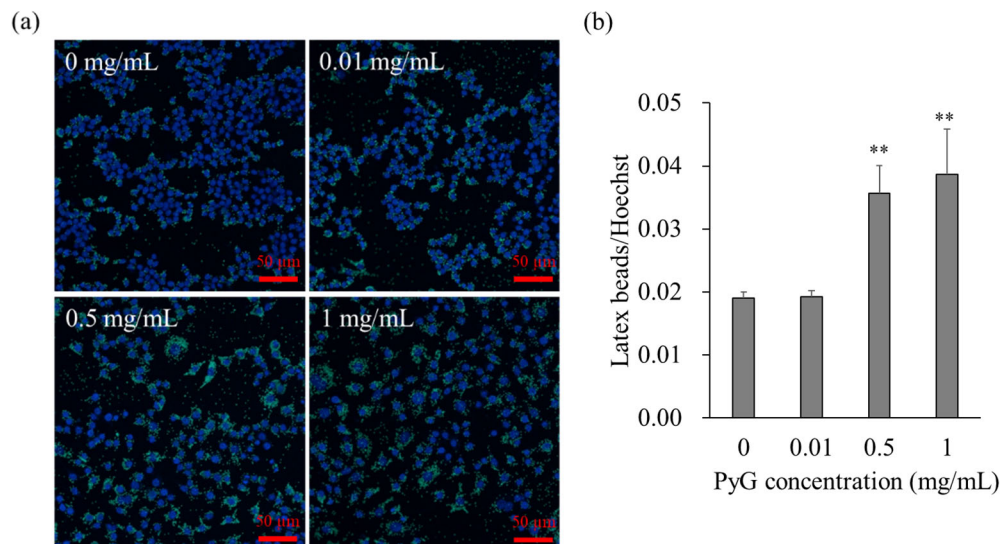


Fig. 2-4 (a) Confocal laser scanning microscopy images and (b) fluorescence intensity after cellular uptake of 1 μm latex beads (10 μg/mL) by RAW264.7 cells. The cells were incubated at 37°C after incubating for 2 h in 0, 0.01, 0.5, and 1 mg/mL of phytoglycogen. Values are represented as mean ± SD (n = 3). (***p* < 0.01, vs. 0 mg/mL)

2.2.4 Particle diameter of phytoglycogen

The particle diameter data (D_{10} , D_{50} , and D_{90}) are presented in **Table 2-1**. As the percentage of ethanol increased, a gradual upward trend in the D_{90} up to 30% was observed. When the ethanol volume ratio in the precursor increased to 40%, the D_{90} increased greatly from 101.1±3.804 nm to 377.5±42.99 nm. Moreover, if ethanol shared half of the solvent composition with water, the particle size of PyG significantly increased in all metrics. Different from the reported diameter of PyG that is around 50 nm, the D_{50} of the PyG molecules enlarged to micro-scale in an ethanol-rich solvent.

Table 2-1 Particle diameter of phytoglycogen in water/ethanol mixed solvent. Values are represented as mean ± SD (n = 3).

Ethanol volume ratio in precursor (%)	Particle diameter (nm)		
	D_{10}	D_{50}	D_{90}
0	30.63±1.365	44.47±1.429	69.13±2.205
10	31.50±2.381	46.87±2.329	77.30±0.700
20	38.57±2.761	57.13±2.108	97.07±4.561
30	36.40±1.386	56.03±2.589	101.1±3.804
40	39.80±7.566	55.00±6.647	377.5±42.99
50	724.6±96.61	1025±155.1	1453±401.6

2.2.5 Size, loading capacity and percentage yield of spray-dried particles

The geometric particle diameter distribution data (D_{10} , D_{50} , D_{90} , and span) are presented in **Table 2-2**. Compared with the untreated materials, all SDPs had smaller particle diameters. On the other hand, a higher ethanol ratio yielded larger particles. The SDPs prepared from RFP and PyG with a 50% ethanol volume ratio had the largest D_{50} at 10.19±0.63 μm . The rifampicin loading capacity and the percentage yield are shown in **Table 2-3**. These two

values had similar outcomes between each group (Loading capacity:~100%; Percentage yield:~70%).

Table 2-2 Dry particle diameter and span of untreated phytoglycogen, untreated rifampicin, and rifampicin/phytoglycogen composite spray-dried particles with varying concentrations of ethanol as solvent. Values are represented as mean \pm SD (n = 3).

Sample	Dry particle diameter (μm)			Span
	D_{10}	D_{50}	D_{90}	
Untreated PyG	13.5 \pm 1.31	28.4 \pm 0.78	44.4 \pm 1.16	1.09
Untreated RFP	4.80 \pm 1.20	33.2 \pm 1.90	72.5 \pm 1.20	2.04
SDPs RFP/PyG, 10% ethanol in precursor	1.28 \pm 0.01	2.98 \pm 0.09	8.68 \pm 0.23	2.48
SDPs RFP/PyG, 20% ethanol in precursor	1.29 \pm 0.05	2.86 \pm 0.10	7.70 \pm 0.42	2.24
SDPs RFP/PyG, 30% ethanol in precursor	1.31 \pm 0.03	3.23 \pm 0.11	11.0 \pm 0.19	3.01
SDPs RFP/PyG, 40% ethanol in precursor	1.30 \pm 0.04	4.00 \pm 0.06	12.6 \pm 0.26	2.83
SDPs RFP/PyG, 50% ethanol in precursor	1.95 \pm 0.03	10.2 \pm 0.63	17.6 \pm 0.94	1.54

Table 2-3 The rifampicin loading capacity and the percentage yield of spray-dried rifampicin/phytoglycogen. Values are represented as mean \pm SD (n = 3).

Sample	SDPs RFP/PyG				
	10	20	30	40	50
Ethanol volume ratio in precursor (%)	10	20	30	40	50
Rifampicin loading capacity (%)	96.7 \pm 4.20	97.4 \pm 2.29	95.9 \pm 4.22	94.5 \pm 4.91	106 \pm 1.37
Percentage yield (%)	74.4 \pm 1.41	67.8 \pm 6.53	66.5 \pm 7.32	73.7 \pm 1.61	70.7 \pm 5.99

2.2.6 Morphology of spray-dried particles

Random images were taken using a scanning electron microscope at 5000 \times magnification (**Fig. 2-5**). The RFP-only SDPs exhibited flake-like shapes (**Fig. 2-5a**). Flake-like and porous RFP–PyG particles are shown in **Fig. 2-5b** to **Fig. 2-5e**. Only the formulation with 50% ethanol (**Fig. 2-5f**) exhibited a peculiar morphology specific to RFP–PyG particles. Small flakes were attached to the uneven surfaces of particles with wrinkled structures. Most flakes had diameters

smaller than 2 μm , whereas the large and wrinkled particles were from 10 to 15 μm in diameter. The morphology is similar to that of the conventional coarse carrier-based formulation, in which the small particles were attached to the larger ones³⁵. However, the SDPs fabricated from RFP and PyG had wrinkled shapes and smaller sizes, compared with the block shapes and larger sizes (50–200 μm) of the conventional lactose carrier^{66,67}.

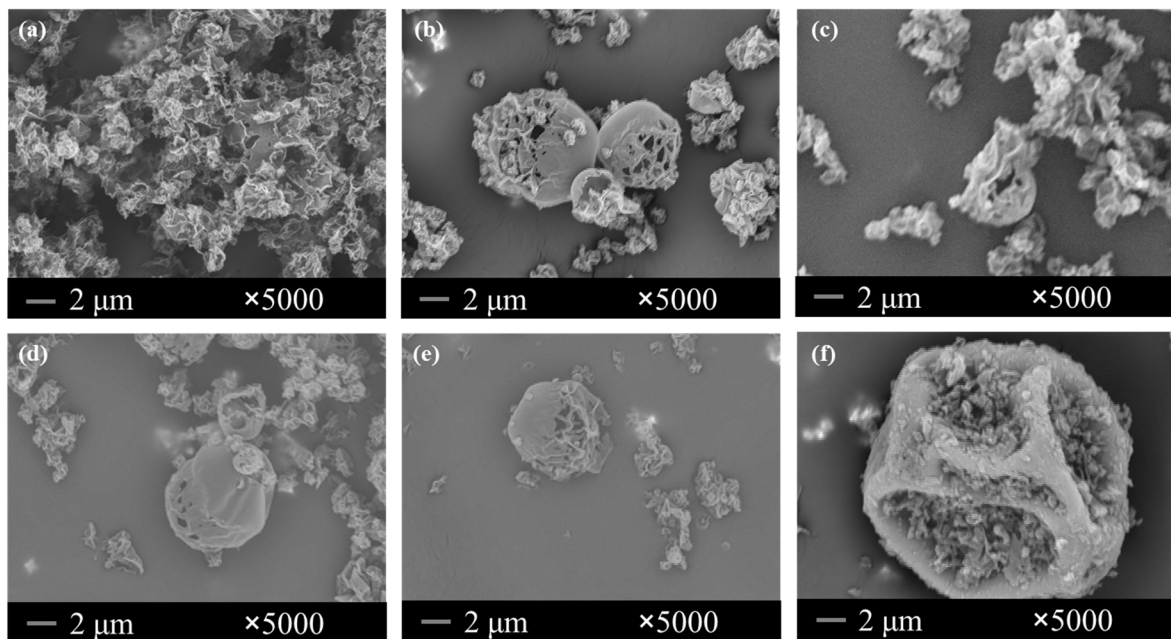


Fig. 2-5 Scanning electron microscope images of spray-dried particles of (a) rifampicin only and rifampicin and phytoglycogen (1/5, w/w) prepared in solvents containing (b) 10%, (c) 20%, (d) 30%, (e) 40%, and (f) 50% ethanol by volume.

2.2.7 Solid state characterization of particles

The PXRD patterns of particles are shown in **Fig. 2-6**. Only the untreated drug and the physical mixture showed crystalline peaks. All other samples exhibited halo PXRD patterns. The DSC curves of samples are shown in **Fig. 2-7**. All samples showed an endothermic peak around 100°C. Untreated RFP also exhibited a sharp endothermic peak at 185°C. Formulations containing PyG showed a peak at various temperatures lower than 160°C.

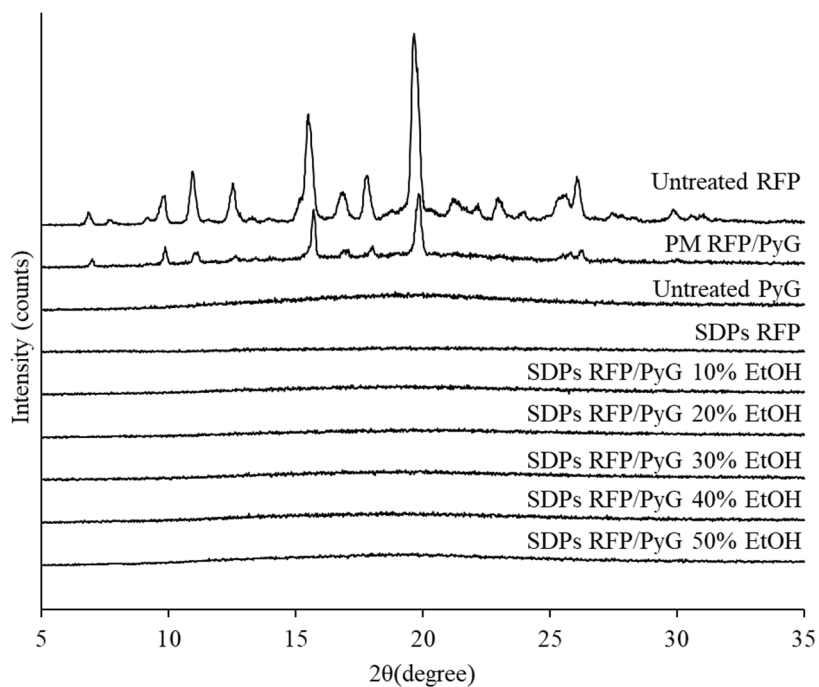


Fig. 2-6 PXR D patterns of untreated rifampicin (RFP), untreated phytyglycogen (PyG), physical mixture (PM) of RFP/PyG (1/5, w/w), spray-dried particles (SDPs) of RFP, and SDPs of RFP/PyG prepared in solvents containing 10%, 20%, 30%, 40%, and 50% ethanol by volume.

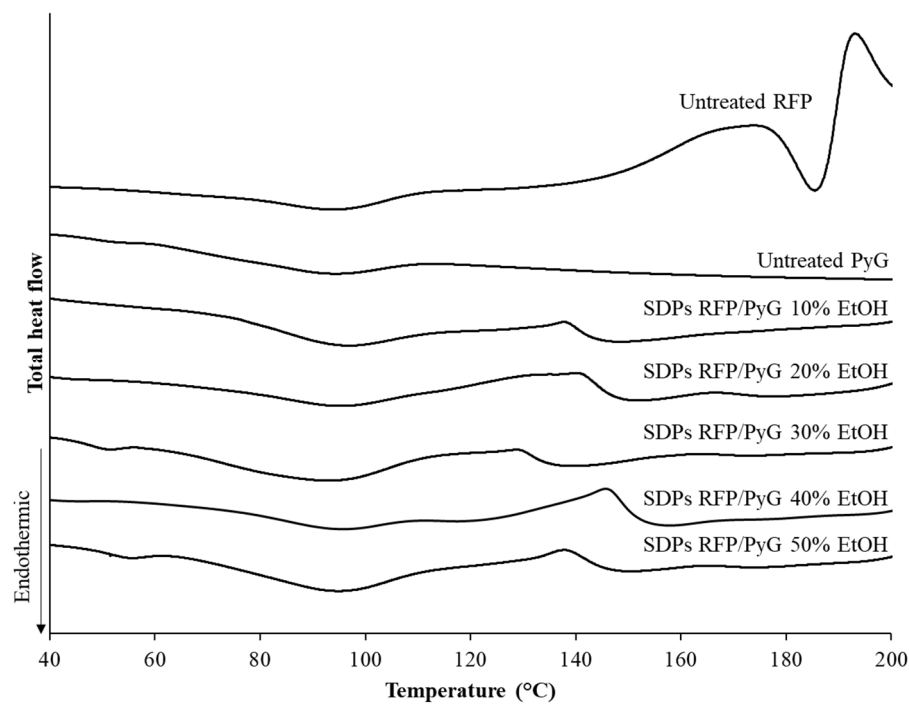


Fig. 2-7 DSC curves of untreated rifampicin (RFP), untreated phytyglycogen (PyG), and spray-dried particles (SDPs) of RFP/PyG prepared in solvents containing 10%, 20%, 30%, 40%, and 50% ethanol (EtOH) by volume.

2.2.8 *In vitro* aerosolization performance of spray-dried particles

Fig. 2-8a shows the deposition behavior of the various types of SDPs at a flow rate of 28.3 L/min. The control groups (RFP/lactose carrier and RFP-only SDPs) were trapped mostly in the shallow stages. This deposition behavior was similar to that of the RFP–PyG SDPs originating from the 10% ethanol precursor. The SDPs prepared from 30% and 40% ethanol precursor deposited a smaller fraction on stage 0, while evenly on stages 1–6 (aerodynamic particle diameter: 1.1–11 μm). Although the SDPs prepared from 20% and 50% ethanol precursor deposited a larger fraction on the deep stages from 5 to 7 (aerodynamic particle diameter: 0.43–2.1 μm), the latter SDPs deposited the highest percentages. **Fig. 2-8b** shows the ED, FPF, and eFPF of all samples. Although the RFP–PyG SDPs originating from 20% ethanol precursor had the highest FPF and the second-highest eFPF, their ED was nearly the lowest. The SDPs originating from 40% ethanol precursor also achieved a high FPF but a low ED. The SDPs originating from 30% ethanol precursor were around the middle of the range in terms of ED, FPF, and eFPF. The SDPs prepared from 50% ethanol precursor were considered the best-performing formulation, with $97.3\pm 2.50\%$ for the ED, $38.9\pm 5.58\%$ for the FPF, and $25.0\pm 1.68\%$ for the eFPF.

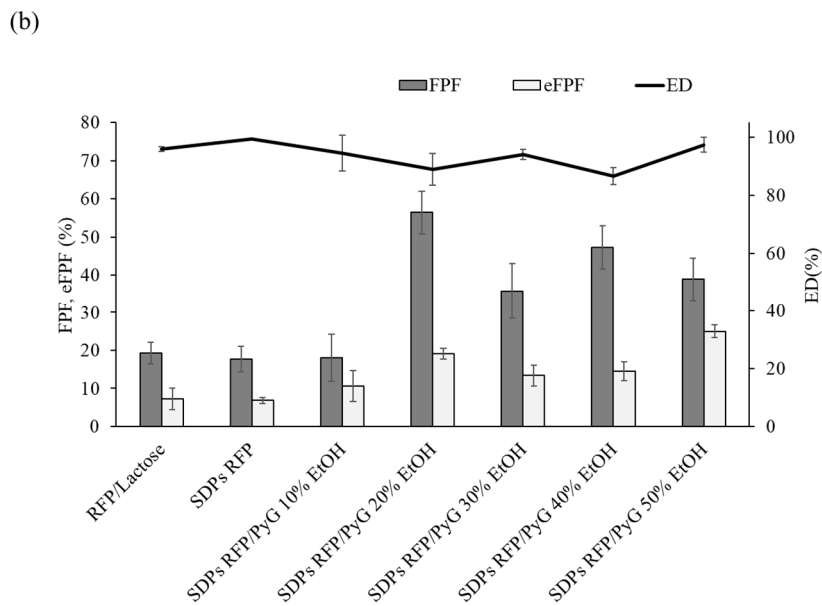
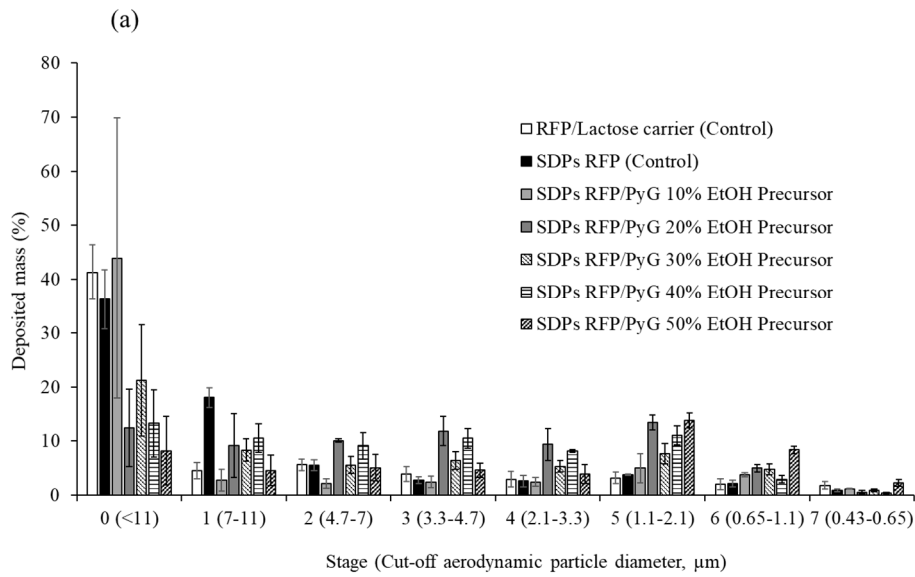


Fig. 2-8 (a) Performance of aerosol dispersions of rifampicin (RFP)/lactose carrier formulation, spray-dried particles (SDPs) of RFP, and SDPs of RFP/phytoglycogen (PyG), as determined using an Andersen cascade impactor at a rate of 28.3 L/min. (b) The emitted dose (ED), fine particle fraction (FPF), and extra-fine particle fraction (eFPF) of RFP/lactose carrier formulation, SDPs of RFP, and SDPs of RFP/PyG were determined using an Andersen cascade impactor at a rate of 28.3 L/min. Values are represented as mean \pm SD (n = 3).

The SEM images of the two types of formulation deposited on each Andersen Cascade Impactor (ACI) stage are displayed in **Fig. 2-9**. The RFP-PyG SDPs originating from 10% and 50% ethanol precursors were compared. The powders originating from 10% ethanol precursor showed a similar particle morphology on each of the stages. Although the particles that reached stage 6 were smaller than the others, the same flake-like and porous shape was retained throughout the ACI. In contrast, the powders originating from 50% ethanol precursor presented different particle shapes when compared with those from the shallow to the deep stages. On stages 0 and 2, large-wrinkled shapes were dominant, and tiny flakes were present on the indented surfaces. On stages 4 and 6, only tiny flakes were visible in the images.

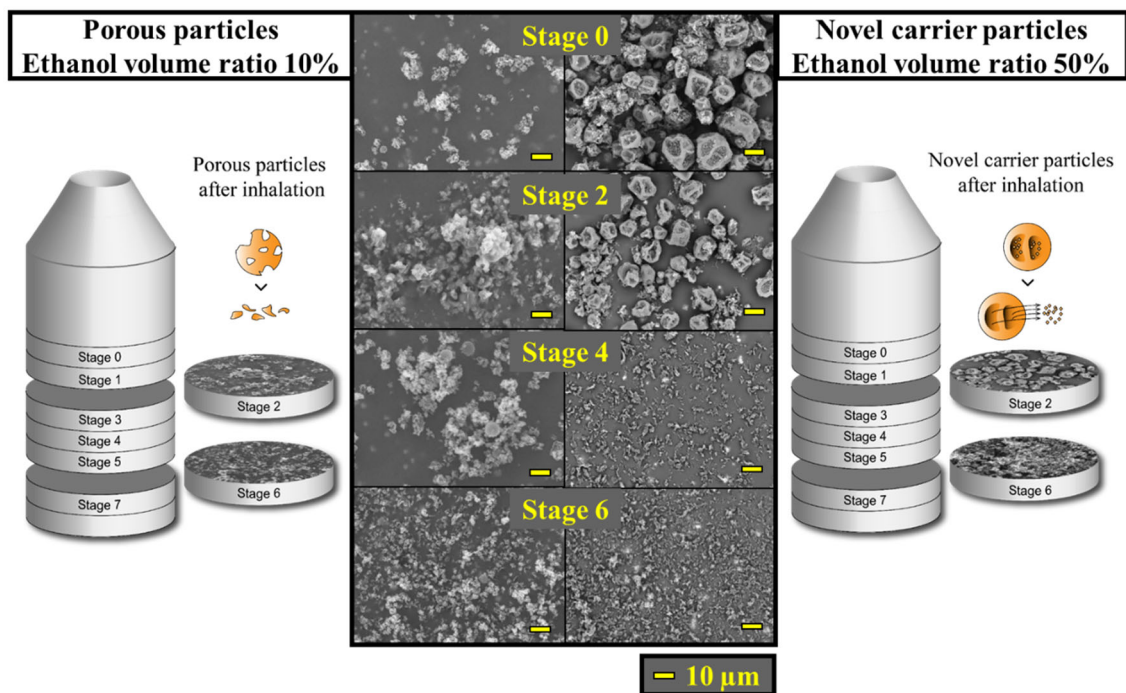


Fig. 2-9 Schematic diagram and scanning electron microscope images of spray-dried particles of rifampicin and phytoglycogen (1/5, v/v) in 10% and 50% ethanol precursor on stages 0, 2, 4, and 6 of the Andersen cascade impactor.

2.3 Discussion

2.3.1 Cell compatibility and the immunostimulatory effect of phytoglycogen

According to the cell viability and cytotoxicity analyses, PyG did not induce cell rupture or death, as there were no considerable differences between the WST-8 assays. PyG was not harmful to A549, Calu-3, or RAW264.7 cells, indicating that PyG showed a high level of safety. The massive molecular weight was favorable for formulation design in terms of flexibility; the hydrophilicity may provide solubilizing effect to poorly water-soluble drugs; the biodegradability and safety are significant for DPI additives for patients to prevent lung injury and pleural thickening⁶⁸. According to its molecular weight, hydrophilicity, biodegradability, and safety, PyG is a potential candidate as a functional excipient for drugs that are aimed for enhanced pulmonary penetration. Moreover, compared with other additives that are usually used in DPI, such as poly(lactic-co-glycolic acid) and lipids of liposomes, PyG showed a great advantage in that there was no cytotoxicity in macrophage-like cells at a high concentration (1 mg/mL)^{69,70}.

The immunomodulatory effects of PyG in RAW264.7 cells are examined. The effect of PyG elevated the gene expression of pro-inflammatory cytokines was found (Fig. 2-3). In addition, the phagocytosis activity of RAW264.7 cells was enhanced by PyG (Fig. 2-4). These results indicate the possibility of an immunostimulatory effect of PyG on macrophages. Macrophages play a key role in host responses to pathogens, including *Mycobacterium tuberculosis*⁷¹. In protecting against pathogen infection, macrophages phagocyte microbial pathogens and secrete various pro-inflammatory cytokines, such as IL-1 β , iNOS, and TNF- α ⁷². Plant polysaccharides have exhibited an immunomodulatory effect by binding to receptors in macrophages, such as toll-like receptor 4 (TLR4), complement

receptor 3, scavenger receptor, and mannose receptors⁷³. On the other hand, exogenous particles such as artificial particles and viruses may also facilitate the immune system via inflammasomes⁷⁴, resulting in the enhanced expression of pro-inflammatory cytokines.

The phagocytosis of particles on macrophages may be elevated by the upregulation of pro-inflammatory cytokines. The enhanced cellular uptake of polystyrene latex beads was confirmed in the presence of higher PyG concentrations (Fig. 2-4). Wijagkanalan *et al.* demonstrated an enhanced cellular uptake of mannosylated liposomes through the mannose receptor-mediated mechanism in alveolar macrophages⁷⁵. Gupta *et al.* showed a TLR4-related immunostimulatory effect on plant polysaccharide-treated RAW264.7 cells⁷⁶. Considering the safety and phagocytosis-enhancing effect of PyG, it has the potential to be adopted as a functional DPI formulation additive. Still, further studies are needed to clarify which receptors bind to PyG to elucidate the PyG-mediated immunostimulatory effects in macrophages.

2.3.2 Effect of solvent composition on phytoglycogen structure

As the properties of precursor before spray drying greatly affect the final SDPs, the particle diameter of PyG in water-ethanol solvents was evaluated using dynamic light scattering (DLS)⁶². The D_{90} of PyG gradually increases with escalating ethanol content up to 30% (Table 2-1). A similar phenomenon was observed in another macromolecular polysaccharide, highly branched cyclic dextrin^{45,47}; however, PyG has a higher particle diameter, which may be due to its higher molecular weight. PyG in water exhibited the smallest particle diameter because sufficient water molecules bound to the glucose unit at the dendron (the end of the dendrimer structure). When the water content in the solvent is

replaced by ethanol up to 40%, the glucose molecules at the dendron unit begin to aggregate, as there are fewer water molecules to provide hydrogen bonding sites⁷⁷. When the water/ethanol volume ratio reaches 50/50, self-aggregation of PyG may be attributed to the glucose units at the dendrons binding to other PyG molecules⁷⁸. However, the hydrodynamic properties of PyG molecules in varying solvents are still unclear, so further investigation is required.

The geometric D_{50} of SDPs greatly increased when the ethanol content in the solvent reached 50% (Table 2-2). This interesting phenomenon is discussed thoroughly in the following sections. The results of loading capacity near 100% indicated the drug was successfully included in each formulation. The percentage yield near 70% also showed the preparation process has a certain value in economic efficiency.

2.3.3 Formation of porous particles

When PyG was combined with a low percentage of ethanol, the product exhibited porous shapes (Fig. 2-5). The reduced density results in smaller aerodynamic particle diameter, so a higher fraction of particles can reach the trachea. The nucleation of RFP may be triggered by the macromolecular polysaccharide in the mixed solvent, ultimately forming porous particles after spray drying. After that, if the dried shell cannot withstand the pressure resulting from the evaporation of the inner solvent, the solid shell fractures to form porous particles^{79,80}. Nandiyanto *et al.* also discussed how the formation of porous particles was affected by the change in heat and mass transfer owing to solute diffusion⁸¹. As described above, PyG exhibited a dendritic structure in aqueous solutions. Moreover, in water-ethanol solvents, RFP molecules may be located near the dendrons of PyG. During solvent evaporation, the formation of an RFP-PyG network may produce porous particles (Fig. 2-9). These porous particles can also be small flake-like particles

under conditions of folding of the shell (due to pressure) or clogging of the inner structure (due to precursor droplets containing a high concentration of PyG). This type of porous particle is advantageous for pulmonary delivery; this is further discussed after the particle formation section.

2.3.4 Formation of large-wrinkled particles

Beyond the porous particles, unique large-wrinkled particles with irregular dents formed when the ethanol volume increased to half of the precursor. As stated above, aggregation between PyG molecules occurred in the highest degree in a 50% ethanol solution. Large-wrinkled particles of approximately 10 μm in diameter were produced when RFP was added. Vehring proposed that a rigid composite shell on the surface of a droplet may form a hollow sphere⁵³. Archer *et al.* also discussed shell formation using the locking point time concept, which is related to the gas phase drying conditions, aerosol droplet composition, and particle formation⁶². The dents on the large particles indicate the buckling of the thin shell^{53,61,82}. This shell buckling behavior was caused by the shrinkage of the droplet even after the accumulation of solute near the air–droplet interface during drying⁶¹. A schematic explanation of the formation of wrinkled particles is shown in **Fig. 2-10**. These large-wrinkled particles were absent in solvent containing less ethanol, indicating the high aggregation degree of PyG was not triggered unless the ethanol volume ratio is high at 50% in the precursor. Crucially, the tiny flakes may be the result of the network between the RFP and non-aggregated PyG; they are similar to the composite particles formed from precursor solvents with ethanol content up to 40%, indicating that PyG in 50% ethanol precursor has a wide particle diameter distribution (Table 2-2).

Nevertheless, the trigger of the robust aggregation of PyG in high ethanol content solvent should be further

investigated using small-angle X-ray scattering (SAXS). The morphology of a single PyG molecule could be investigated by SAXS. As mentioned in Section 1.5, PyG has a dendritic structure if it is dispersed in water. The structure of the dendrimers may change in a poor solvent-rich environment due to the aggregation of dendrons to form a packed PyG molecule⁷⁷. The hydrophilic outer layer may then facilitate the accumulation of PyG molecules to form a liquid-solid phase transition that settles a precipitate. Thus, one of the possibilities to explain the origin of large-wrinkled particles is precipitation. Moreover, the critical condition for the formation of large-wrinkled PyG particles may also be discovered by future experiment sets, such as adjusting the solvent ethanolic content in a smaller interval, with a change in PyG concentration in the spray-drying precursor as a second variable.

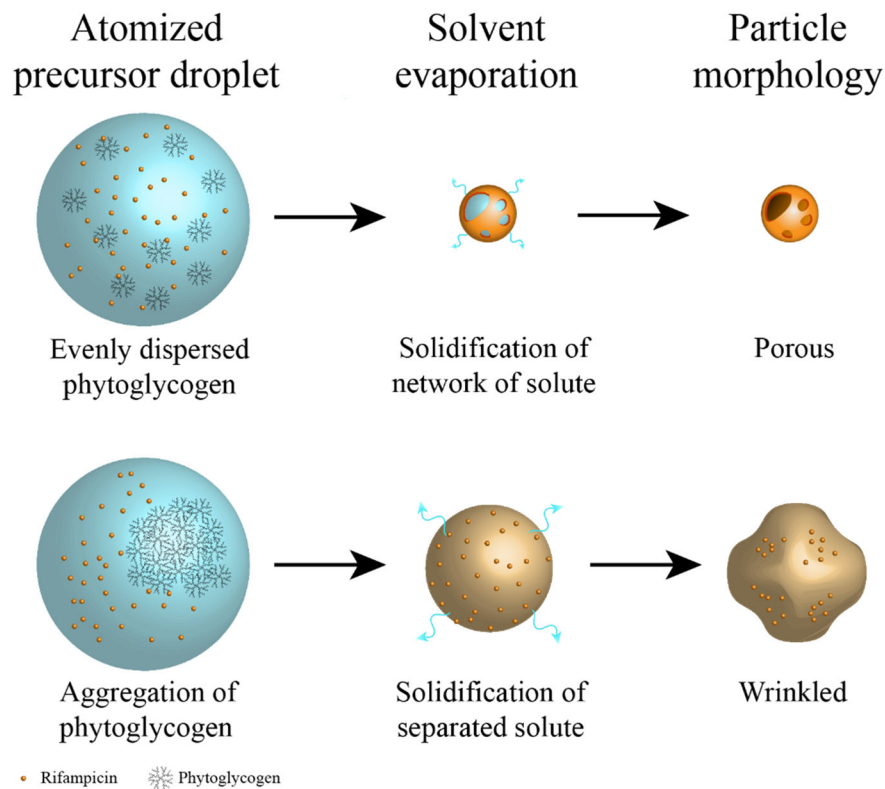


Fig. 2-10 Schematic diagram of the formation of porous and wrinkled particles.

2.3.5 Particle morphology alters deposition behavior

To test its feasibility as an excipient for DPI formulations, the ability of PyG to produce inhalable particles was studied. Regarding the RFP-only SDPs, although the primary particle size was small, the secondary particle size resulted from agglomeration; these particles were deposited into the shallow stages of the ACI. This result also shows the importance of carrier additives. SDPs prepared from 20% and 40% ethanol precursors had the highest FPF. FPF is derived from fine particle dose; this kind of respirable fraction has been used widely in the industrial field to describe the degree of particles penetrating and depositing within human lungs²⁰. Considering various aspects such as morphology and density, particles with lower sizes are not equivalent to fine particles⁵³. The high FPF values obtained in the formulations indicate higher fractions of particles that have a greater chance to deposit on effective sites per dosage²⁰. Nonetheless, low FPF value may risk the patient for side effects as drugs were not delivered to a suitable region such as the mouth and the throat⁸³. However, the formulations both had low EDs. The low ED resulted from large agglomerates that failed to exit the capsule, whereas these agglomerates were excluded in the FPF calculation¹⁶. Powders that fail to exit the capsule may lead to uneven doses. As shown in Fig. 2-8a, the deposition behavior of the formulation that originated from 50% ethanol precursor was unique. Compared to the deposited mass on stage 4, that on stage 5 was three times higher, and that on stage 6 was double the mass. No other candidate deposited more than 5% of the mass on stage 6.

As summarized in Fig. 2-9, taking the mixture with 10% ethanol as an example, the porous particles were distributed relatively evenly on the ACI stages according to the diameter distribution. In addition, the novel carrier

containing large-wrinkled particles showed a unique deposition behavior. Tiny flake-like particles were initially attached to the surface of the large-wrinkled particles. This feature suppressed the agglomeration of the small particles. During inhalation, the wrinkled particles were able to reach the trachea-equivalent ACI stage. At that point, small particles on the large-wrinkled particle surface started to detach due to turbulence; therefore, a higher number of small particles could be delivered to the lower stages (5–7) of ACI. As previously mentioned, the tiny particles may be derived from the network of non-aggregated PyG and RFP. By delivering more composite particles to the alveoli-equivalent ACI stages, RFP can directly reach the infected alveolar macrophages to exert its antibacterial effect. At the same time, PyG can induce the immunostimulatory effect shown in the studies in RAW 264.7 cell lines. Three advantages over the conventional carrier method can be observed from this phenomenon: (1) improved drug and additive uniformity, (2) reduced side effects of carrier particles, and (3) enhanced alveolar delivery of drugs. With the conventional method, adhesion of the mixture of the coarse carrier and micronized drug gave rise to a dose uniformity issue¹⁴. Because of their size (50–200 μm) and dose (drug/carrier, 1/67.5, w/w), coarse carrier particles are usually not deposited further than the patient's throat, leading to side effects such as coughing and bronchoconstriction⁵⁵. The alveoli were also unreachable for these drug particles because of their lack of penetration^{54,55}. The comparison in aerosolization performance between the conventional RFP/lactose carrier formulation and the novel carrier particle formulations was exhibited in Fig. 2-8. The novel carrier particles improve the penetration of drug–additive composite particles, resulting in an immunostimulatory effect on macrophages and a potential enhancement of the therapeutic effect.

2.4 Summary

Considering the lack of choice in DPI formulation additives for particle design, a new candidate, PyG, is proposed for pharmaceutical research. It does not show cytotoxicity in A549, Calu-3, and RAW264.7 cell lines. This novel carrier also showed a phagocytic activity-enhancing effect on macrophage-like cells, indicating the usefulness of PyG reaching the alveoli. By spray drying, porous particles and large-wrinkled particles with enhanced inhalation performance were produced. Because of the carrier effect of the large-wrinkled particles, an outstanding alveolar delivery ability was attained.

Chapter 3 Optimization of spray-drying parameters for preparation of formulations with enhanced alveolar delivery

3.1 Introduction

The SDP properties are affected by numerous parameters in the preparation process⁸⁴. Properties of precursor including material composition, material ratio, solid content, and solvent composition are also determining factors. Thus, a statistical approach, DoE, has been popular among scientists who are interested in optimizing preparation parameters^{85,86}. This can also help to identify critical process parameters and their interaction for desirable outcomes⁸⁷. Compilation of contour plots generated from response surface methodology (RSM) would determine a design space, for the convenient and rational preparation of desirable products⁸⁸.

PyG and LEU were adopted as additives of DPI formulations containing levofloxacin (LVFX). LVFX was anticipated to present the best response against bacterial diseases if delivered directly into the lungs. LEU is an amino acid, which can enhance aerosolization and suppress particle adhesion due to its hydrophobicity and weak surfactant property^{89,90}. Amino acids diffuse to the surface of the droplet during spray-drying on behalf of its hydrophobicity, thus lowering the chance of agglomeration of particles by hindering the hygroscopic effect. The use of LEU can effectively reduce the adhesion of particles due to a decrease of surface energy, and thus enhances the delivery of API deep into the lungs^{2,42,91}.

A three-factor-three-level face-centered central composite design was selected as the model to perform the DoE for two purposes: 1) to understand the influence in responses of factors; 2) to optimize factors for qualified

outcomes. Inlet temperature (X_1), feed flow rate (X_2), and gas flow rate (X_3) were selected as factors of the model (**Fig. 3-1a**). The actual experimental values were listed in **Table 5-2-1** in **Section 5.2.6**. These factors have been investigated as critical parameters to optimize particle properties, such as size and inhalation properties^{88,92-95}. Other spray-drying parameters, such as nozzle type and aspiration, were fixed to suppress the number of experimental runs. A sequence of designed experiments was conducted (**Fig. 3-1b**). Five response variables (Y_1 : ED, Y_2 : FPF, Y_3 : eFPF, Y_4 : percentage yield, and Y_5 : aerodynamic diameter) with respect to the inhalation performance or manufacturing efficiency were included in the analysis.

The purpose of this chapter is to design LVFX-containing SDPs with enhanced deep lung delivery ability; hence, to showcase the usefulness of the DoE in optimizing DPI formulations based on macromolecular polysaccharides. The influence of process variables on the properties of the products was also investigated. The performance and validity of the optimization design were evaluated to ensure the credibility of the statistical approach.

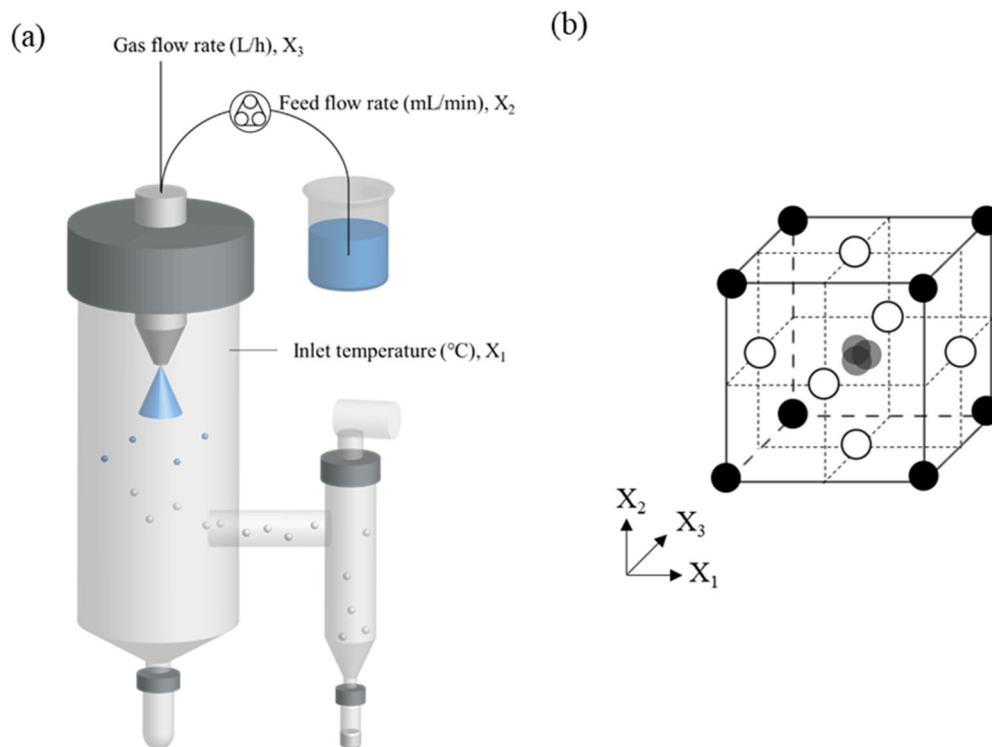


Fig. 3-1 (a) The spray-drying parameters selected as factors of the design of experiments. (b) A face-centered central composite design model for the design of experiments. (Black dots, corner points; white dots, axial points; gray dots, center points)

3.2 Results

3.2.1 Particle morphology of spray-dried particles

The SEM image of spray-dried LVFX is shown in **Fig. 3-2a**. Other than spheres, the SDPs of LVFX also have needle-like or other irregular shapes. After the addition of PyG into the formulation, almost all SDPs were in deflated ball shapes (**Fig. 3-2c**), which was similar to those of the spray-dried PyG (**Fig. 3-2b**).

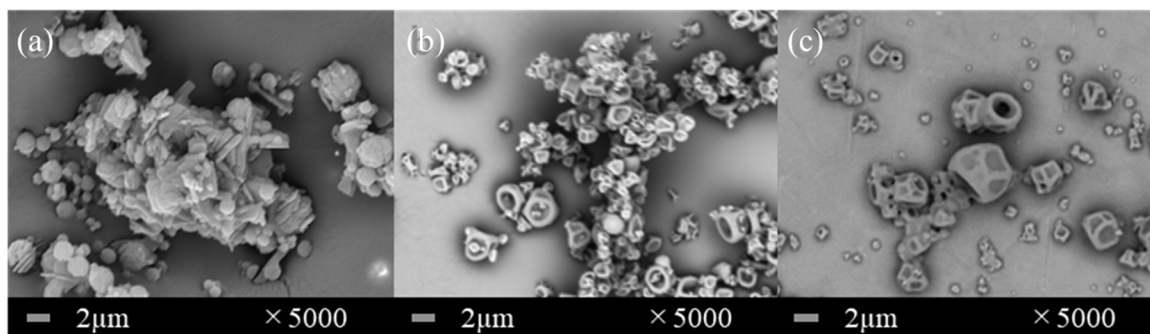


Fig. 3-2 SEM images of (a) spray-dried levofloxacin particles, (b) spray-dried phytoglycogen particles, and (c) spray-dried levofloxacin/phytoglycogen (1/5, w/w) particles.

3.2.2 Analysis of the central composite design model

The most suitable formulation of LVFX/PyG/LEU was evaluated prior to the optimization of spray-drying parameters. The outcomes of jet-milled LVFX, or powders with varying solid compositions, are shown in **Table 3-1**. The aerosolization performance of samples is also exhibited in **Fig. 3-3**. The results of the ACI inhalation test revealed that the jet-milled LVFX powders contain the least number of fine particles. Spray-dried LVFX particles resulted in an FPF lower than 20%, a low ED, and a low percentage yield. The low ED may be due to the occurrence of static electricity charges among small particles. The best formulation of LVFX/PyG/LEU was 1/5/1 by weight; thus, the formulation ratio was adopted in the subsequent preparation processes.

Table 3-1 Response values of levofloxacin jet-milled powders, levofloxacin spray-dried particles, levofloxacin/phytoglycogen spray-dried particles, and levofloxacin/phytoglycogen/leucine spray-dried particles. (Y_1 = emitted dose, Y_2 = fine particle fraction, Y_3 = extra-fine particle fraction, Y_4 = Percentage yield)

Powder type	Solid composition ratio			Response			
	Levofloxacin	Phytoglycogen	Leucine	Y_1 , %	Y_2 , %	Y_3 , %	Y_4 , %
Jet-milled	1	0	0	85.6	12.5	2.6	-
Spray-dried	1	0	0	67.0	16.0	3.3	20.5
Spray-dried	1	5	0	97.9	25.5	2.6	66.7
Spray-dried	1	10	0	99.1	24.8	2.1	60.2
Spray-dried	1	5	1	96.1	43.4	4.8	64.3
Spray-dried	1	10	1	98.5	36.0	3.8	56.6

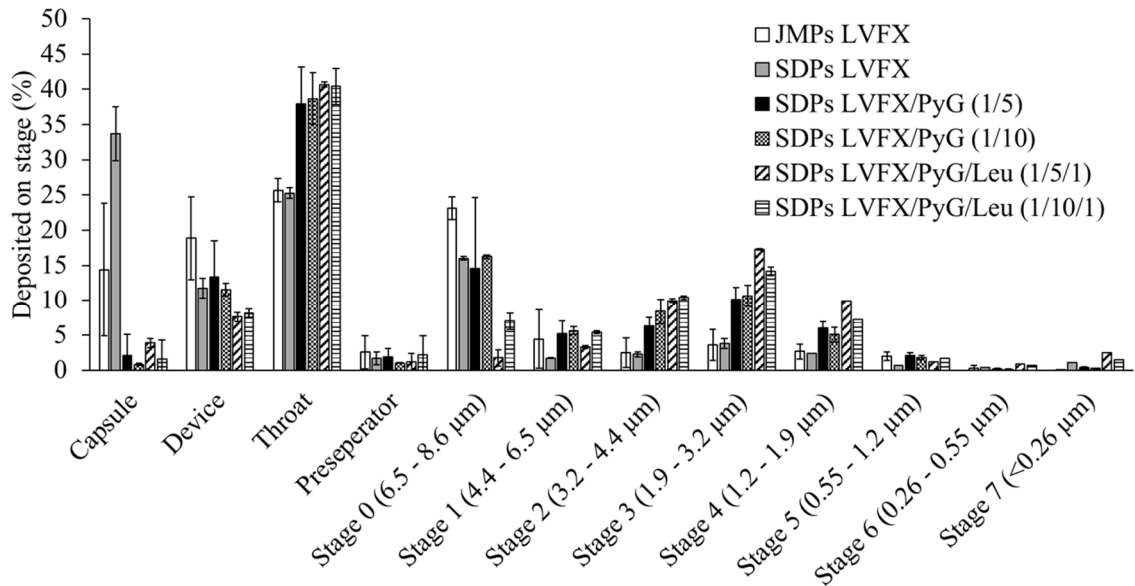


Fig. 3-3 The aerosol dispersion performance of jet-milled particles (JMPs) of levofloxacin (LVFX), spray-dried particles (SDPs) of LVFX, SDPs of LVFX/phytoglycogen (PyG), and SDPs of LVFX/PyG/leucine (LEU). Values are represented as mean \pm SD (n = 3).

The geometric particle size and the bulk density in **Table 3-2** were implied to calculate the aerodynamic diameter. All samples shared the same true density owing to their consistent formulations. The true density of the particles evaluated by the gas pycnometer was 1.48 g/cm^3 . The true density was divided by the bulk density of each spray-drying run to obtain the value of ρ_p in Eq. 1-1. The aerodynamic diameter (Y_5) was then calculated by multiplying the square-rooted value of ρ_p by the D_{50} .

Table 3-2 Geometric particle diameter and bulk density of the particles prepared by the spray-drying runs. (X_1 = inlet temperature, X_2 = feed flow rate, X_3 = gas flow rate)

#	Process			Result				
	$X_1, ^\circ\text{C}$	$X_2, \text{mL/min}$	$X_3, \text{L/h}$	Geometric particle diameter ($D_{50}, \mu\text{m}$)				Bulk density (g/cm^3)
				D_{10}	D_{50}	D_{90}	Span	
1	120	1.5	300	1.971	6.241	11.29	1.493	0.149
2	180	1.5	300	2.521	7.526	13.07	1.402	0.121
3	120	7.5	300	1.713	5.354	10.04	1.555	0.164
4	180	7.5	300	2.347	7.018	12.37	1.428	0.141
5	120	1.5	670	0.630	1.210	2.275	1.360	0.137
6	180	1.5	670	0.708	1.346	2.442	1.288	0.110
7	120	7.5	670	0.678	1.344	2.566	1.405	0.202
8	180	7.5	670	0.736	1.480	2.815	1.405	0.166

9	120	4.5	485	0.805	1.748	3.404	1.487	0.183
10	180	4.5	485	0.901	1.991	4.084	1.599	0.132
11	150	1.5	485	0.879	1.763	3.285	1.365	0.120
12	150	7.5	485	0.909	2.015	4.164	1.615	0.138
13	150	4.5	300	1.356	5.380	11.98	1.975	0.130
14	150	4.5	670	0.691	1.339	2.477	1.334	0.181
15	150	4.5	485	0.940	2.057	4.198	1.584	0.126
16	150	4.5	485	0.907	1.988	4.055	1.583	0.154
17	150	4.5	485	0.977	2.229	4.796	1.713	0.146

The experimental response values (ED, FPF, eFPF, percentage yield, and aerodynamic diameter) of the model-generated spray-drying runs are listed in **Table 3-3**. The results were compiled into the software for subsequent ANOVA analysis to generate response surface reports. Parameters indicating the accuracy and fitting of the model are shown in **Table 3-4**. The *p*-values of all responses in the model were lower than 0.05, indicating the statistically significant differences in the model. The values in the lack of fit in all responses were higher than 0.05, indicating that the DoE model was a good fit. To detect the suitability of the model, the coefficient of determination of R^2 was evaluated. R^2 values above 0.8 show a good fit of the model.

Table 3-3 Face-centered central composite design and mean values of their corresponding responses. (X_1 = inlet temperature, X_2 = feed flow rate, X_3 = gas flow rate, Y_1 = emitted dose, Y_2 = fine particle fraction, Y_3 = extra-fine particle fraction, Y_4 = Percentage yield, Y_5 = Aerodynamic particle diameter)

#	Process			Response				
	$X_1, ^\circ\text{C}$	$X_2, \text{mL/min}$	$X_3, \text{L/h}$	$Y_1, \%$	$Y_2, \%$	$Y_3, \%$	$Y_4, \%$	$Y_5, \mu\text{m}$
1	120	1.5	300	99.5	18.5	2.3	57.8	1.98
2	180	1.5	300	98.5	14.4	1.6	65.7	2.15
3	120	7.5	300	98.2	14.8	1.1	39.0	1.78
4	180	7.5	300	98.0	17.9	1.6	40.1	2.17
5	120	1.5	670	84.7	34.8	9.6	46.7	0.37
6	180	1.5	670	69.0	15.9	7.1	47.4	0.37
7	120	7.5	670	89.5	50.2	6.4	63.2	0.50
8	180	7.5	670	85.9	36.8	8.6	61.6	0.50
9	120	4.5	485	96.1	43.4	4.8	68.6	0.62
10	180	4.5	485	95.7	40.6	7.1	69.9	0.60

11	150	1.5	485	91.1	21.0	8.5	62.1	0.50
12	150	7.5	485	96.1	35.3	7.0	69.5	0.62
13	150	4.5	300	98.4	17.0	1.9	38.3	1.60
14	150	4.5	670	77.6	22.3	10	47.2	0.47
15	150	4.5	485	95.6	41.8	4.6	76.6	0.60
16	150	4.5	485	93.2	44.4	7.7	69.8	0.64
17	150	4.5	485	97.2	46.3	6.9	70.5	0.70

Table 3-4 Fitted model terms for measured responses. (* $p < 0.05$)

Term	Response				
	Emitted dose (Y ₁)	Fine particle fraction (Y ₂)	Extra-fine particle fraction (Y ₃)	Percentage yield (Y ₄)	Aerodynamic diameter (Y ₅)
Model	0.0004*	0.0119*	0.0052*	0.0050*	0.0000*
Lack of fit	0.3876	0.0850	0.7453	0.2940	0.0845
R ²	0.9600	0.8904	0.9153	0.9161	0.9799
Adjusted R ²	0.9085	0.7495	0.8064	0.8083	0.9541
Predicted R ²	0.5186	0.4432	0.4274	0.5891	0.8501
SD	2.5500	6.4642	1.3253	5.5456	0.1443

The predicted versus reference scatter is plotted in **Fig. 3-4**. The plot shows that the better the fit, the closer the dots on a straight line. The selected predicted Y-value from the model is plotted against the reference Y-value. Other than those for FPF, all slopes were above 0.9. Offset is the intercept of the line with the Y-axis when the X-axis is set to zero. The correlations between the predicted and reference values in the plot of all responses were higher than 0.94. Root mean square error of deviation (RMSED) is also included near the lines. Standard error of deviation (SED) is the RMSED corrected for bias. It is the average value over all points that either lie systematically above (or below) the regression line. The data sets of extra-fine particle fraction and aerodynamic particle diameter had the least SED, indicating their experimental results lay close to the predicted values.

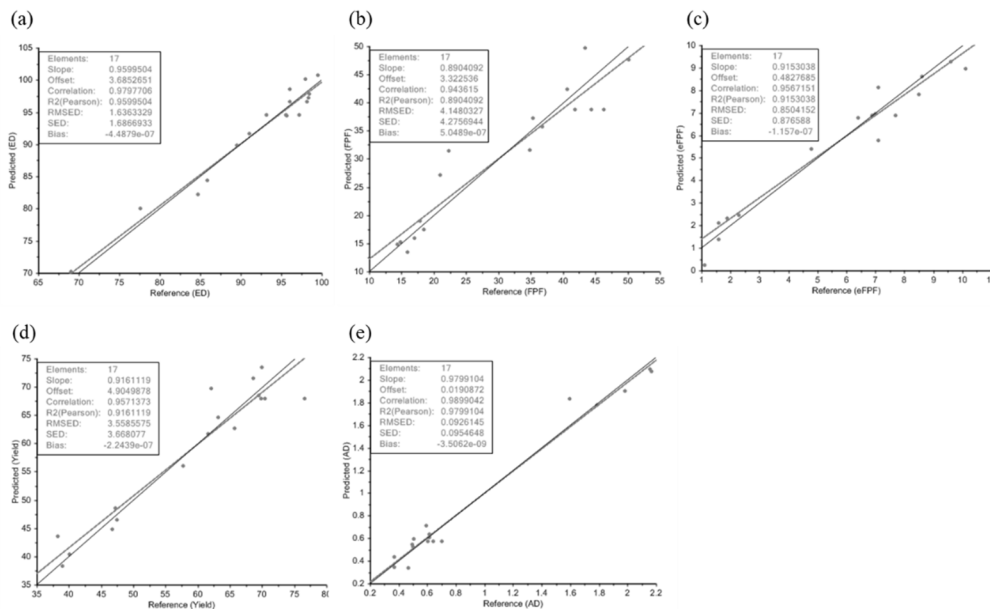


Fig. 3-4 Predicted versus reference scatter plot of (a) emitted dose, (b) fine particle fraction, (c) extra-fine particle fraction, (d) percentage yield, and (e) aerodynamic particle diameter. The blue line indicates the regression line, and the black line denotes the target line.

Calculated β -coefficients and p -values of each term on the responses are shown in **Table 3-5**. When writing a regression model (**Eq. 5-2-1**) for each response, non-significant terms were removed to attain a better fit. The regression models **Eq. 3-1** to **Eq. 3-5** correspond to the responses ED, FPF, eFPF, percentage yield, and aerodynamic diameter, respectively.

$$\text{Emitted dose (\%)} = 94.53 - 2.09X_1 + 2.49X_2 - 8.59X_3 - 2.26X_2^2 + 2.94X_3^2 - 5.92X_2X_3 \quad \text{Eq. 3-1}$$

$$\text{Fine particle fraction (\%)} = 38.77 + 5.04X_2 + 7.74X_3 - 15.07X_2X_3 \quad \text{Eq. 3-2}$$

$$\text{Extra-fine particle fraction (\%)} = 6.88 + 3.33X_3 \quad \text{Eq. 3-3}$$

$$\text{Percentage yield (\%)} = 67.91 + 9.39X_3^2 - 21.86X_2X_3 \quad \text{Eq. 3-4}$$

$$\text{Aerodynamic diameter (\mu m)} = 0.57 - 0.75X_3 + 0.51X_2X_3 \quad \text{Eq. 3-5}$$

Table 3-5 Calculated β -coefficients and p -values of each term on the responses. ($*p < 0.05$)

Terms	Response									
	Emitted dose (Y_1)		Fine particle fraction (Y_2)		Extra-fine particle fraction (Y_3)		Percentage yield (Y_4)		Aerodynamic diameter (Y_5)	
	β -coefficient	p -value	β -coefficient	p -value	β -coefficient	p -value	β -coefficient	p -value	β -coefficient	p -value
β_0	94.5267		38.770		6.876		67.909		0.5743	
X_1	-2.0900	0.0359*	-3.6100	0.1207	0.1800	0.6805	0.9400	0.6085	0.0534	0.2802
X_2	2.4900	0.0176*	5.0400	0.0431*	-0.4400	0.3287	-0.6300	0.7300	0.0187	0.6947
X_3	-8.5900	0.0000*	7.7400	0.0068*	3.3300	0.0001*	2.5200	0.1939	-0.7485	0.0000*
X_1^2	1.6125	0.1168	1.5875	0.5097	0.7375	0.1595	-1.1375	0.5800	0.0266	0.6185
X_2^2	-2.2625	0.0404*	-3.9125	0.1306	-0.0125	0.9795	-1.2375	0.5480	-0.0698	0.2135
X_3^2	2.9375	0.0139*	4.5625	0.0861	-0.0625	0.8976	9.3875	0.0020*	0.0551	0.3157
X_1X_2	1.9782	0.2447	7.2768	0.1079	-1.2831	0.1570	4.6352	0.2136	0.0859	0.3622
X_1X_3	-0.3218	0.8422	-6.5732	0.1400	0.5169	0.5435	1.1852	0.7368	0.0400	0.6637
X_2X_3	-5.9218	0.0067*	-15.073	0.0066*	-1.2331	0.1716	-21.865	0.0003*	0.5130	0.0007*

3.2.3 Influence of inlet temperature, feed flow rate, and gas flow rate on outcomes

Contour plots were generated from the experimental data (**Figs. 3-5 to Fig. 3-9**). Each contour plot shows the influence of two independent variables on the response outcome if the remaining variable is fixed. The coded value of either -1, 0, or 1 of the fixed independent variables was selected if it enabled the best outcome. Only the coded value of the fixed independent variable in **Fig. 3-5a** was selected in a different manner, owing to the generation of the design space in **Section 3.2.5**. The X- and Y- axes of the contour plots were the experimental values of the independent variables. The color intensity of the contour plot represents the level of response outcomes; bluish color represents a low response level and reddish color represents the opposite. Numerical values of outcomes are also marked in each plot.

Contour plots showing the influence of independent variables on ED are shown in **Fig. 3-5**. Under 120°C inlet temperature, the gas flow rate was the determining factor for ED; the feed flow rate parameter had a small influence (**Fig. 3-5a**). Lower gas flow rates obtained a higher ED value. If the feed flow rate was set at 7.5 mL/min, a lower gas flow rate could lead to a higher ED (**Fig. 3-5b**). Moreover, the higher ED is obtained when the temperature is at the two extremes of the values tested when the gas flow rate is slightly below 0 in the coded value. In the case of the gas flow rate higher than the middle level, the ED would be slightly favorable at about 150°C. When the gas flow rate was fixed at a low level, the ED varied in a small degree at $\pm 3.4\%$ (**Fig. 3-5c**).

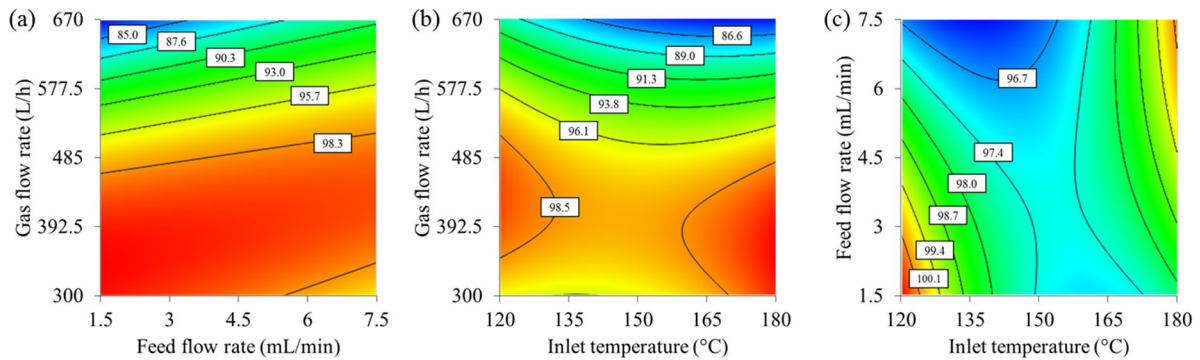


Fig. 3-5 Contour plots of the emitted dose as a function of (a) feed flow rate and gas flow rate with an inlet temperature of 120°C, (b) inlet temperature and gas flow rate with a feed flow rate of 7.5 mL/min, and (c) inlet temperature and feed flow rate with a gas flow rate of 300 L/h.

The influence on the degree of fine particles of factors is shown in **Fig. 3-6**. When the inlet temperature was 120°C, the high FPF region appeared as an oval shape with the feed and gas flow rates as variables (**Fig. 3-6a**). By fixing the feed flow rate at 7.5 mL/min, a high FPF could only be achieved when the gas flow rate was set around 577.5 L/h (**Fig. 3-6b**). A weak quadratic relationship between inlet temperature and FPF was found since higher FPF values could be obtained at both high and low limits of the inlet temperature factor. By setting the gas flow rate at 670 L/h, high FPF values were obtained only when the inlet temperature was set at a low limit and the feed flow rate was set at the middle level or a high limit (**Fig. 3-6c**).

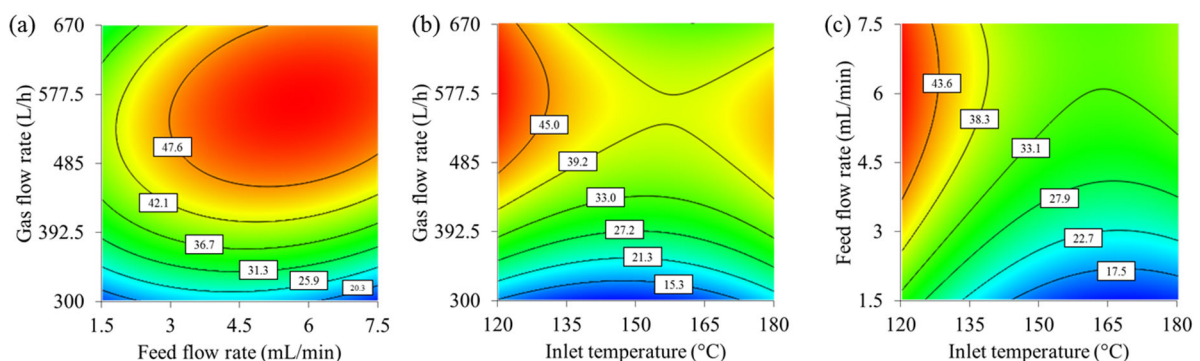


Fig. 3-6 Contour plots of the fine particle fraction as a function of (a) feed flow rate and gas flow rate with an inlet temperature of 120°C, (b) inlet temperature and gas flow rate with a feed flow rate of 7.5 mL/min, and (c) inlet temperature and feed flow rate with a gas flow rate of 670 L/h.

Fig. 3-7 shows three contour plots, taking eFPF as the dependent variable. A high level of eFPF could only be obtained when the gas flow rate was set at a high level (**Figs. 3-7a&b**). Inlet temperature and feed flow rate had a minimal influence on the extra-fine particle fraction. When the gas flow rate was set at a high level, the powder products had a high eFPF value in the entire contour plot (**Fig. 3-7c**).

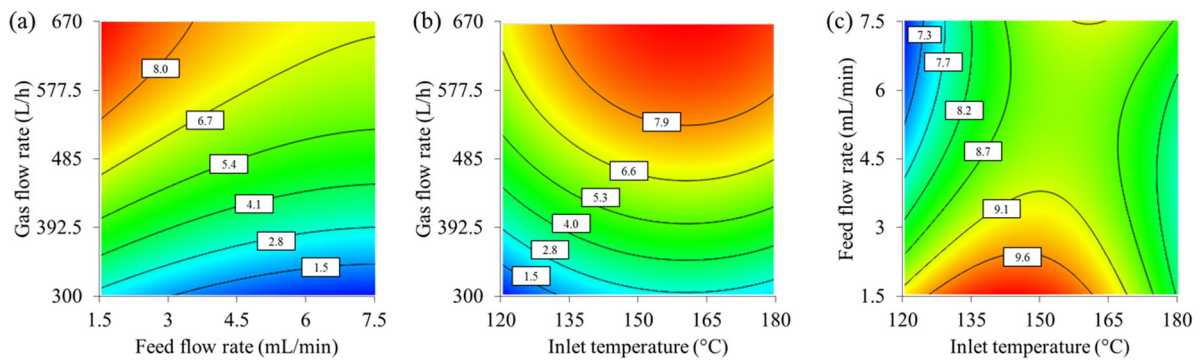


Fig. 3-7 Contour plots of the extra-fine particle fraction as a function of (a) feed flow rate and gas flow rate with an inlet temperature at 120°C, (b) inlet temperature and gas flow rate with a feed flow rate of 7.5 mL/min, and (c) inlet temperature and feed flow rate with the gas flow rate at 670 L/h.

The relationship between percentage yield and spray-drying parameters is illustrated in **Fig. 3-8**. The highest percentage yield could be obtained by setting the gas flow rate at the middle level when the inlet temperature was 120°C (**Fig. 3-8a**). The feed flow rate had minimal influence in this situation. A gas flow rate at the middle level could also facilitate yield under conditions of a fixed feed flow rate; however, inlet temperature had a minor impact (**Fig. 3-8b**). **Fig. 3-8c** showed that a high feed flow rate was essential for obtaining a higher percentage yield whenever the gas flow rate was fixed at a high level.

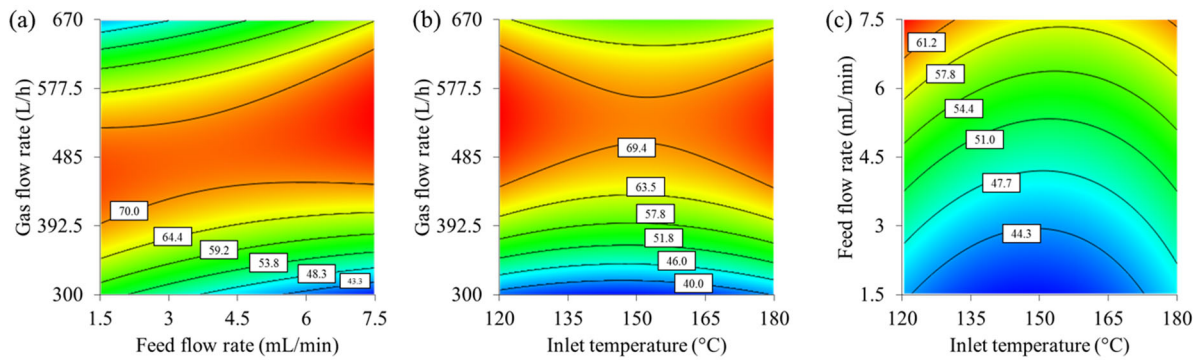


Fig. 3-8 Contour plots of percentage yield as a function of (a) feed flow rate and gas flow rate with an inlet temperature of 120°C, (b) inlet temperature and gas flow rate with a feed flow rate of 7.5 mL/min, and (c) inlet temperature and feed flow rate with a gas flow rate of 670 L/h.

Response surfaces of aerodynamic particle diameter are shown in **Fig. 3-9**. Contour plots in **Figs. 3-9a&b** show a similar pattern, indicating a vast influence of gas flow rate on aerodynamic diameter. The inlet temperature and feed flow rate had little impact compared with the rate of gas flow. If the gas flow rate was set at the high limit, as shown in **Fig. 3-9c**, an inlet temperature at the middle point and a low feed flow rate will reduce the aerodynamic diameter of particles.

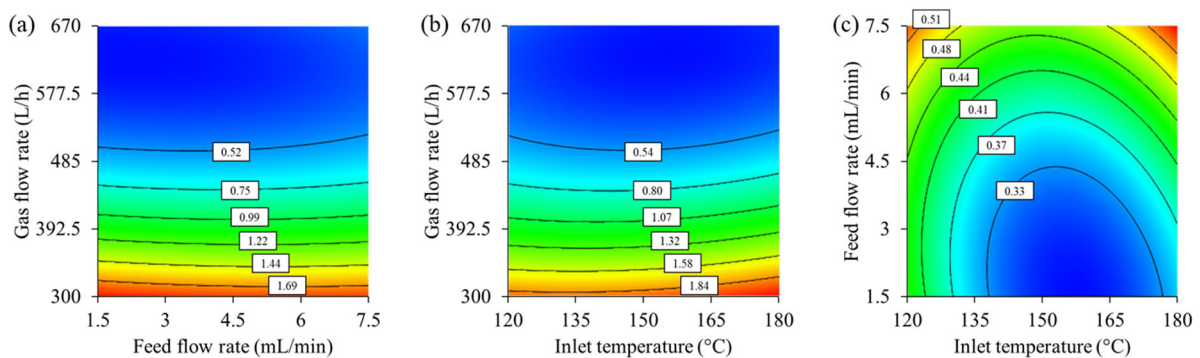


Fig. 3-9 Contour plots of the aerodynamic particle diameter as a function of (a) feed flow rate and gas flow rate with an inlet temperature of 120°C, (b) inlet temperature and gas flow rate with a feed flow rate of 7.5 mL/min, and (c) inlet temperature and feed flow rate with a gas flow rate of 670 L/h.

3.2.4 Optimization of experimental variables – the design space

Target levels of ED, FPF, eFPF, and percentage yield were set to facilitate the optimization of process parameters. Kugler *et al.* reported that the marketed DPI, Turbuhaler[®], achieved an ED of 80%⁹⁶. For a stretched goal, an ED above 90% was aimed in the current optimization. The FPF of marketed DPI formulations was reported to be around 30%⁹⁷. To establish the target eFPF, Boer *et al.* revealed that the submicron fractions of some marketed DPIs, including Turbuhaler[®], Diskus[®], and Elpenhaler[®], were less than 5%⁹⁸. Herein, a target to prepare DPI formulations with eFPF values that are higher than 5% was set. The product yield was aimed above 70%, which contributed to a highly economically effective manufacturing process. To summarize, the target levels were set as follows: ED above 90%, FPF above 40%, eFPF above 5%, and percentage yield above 70%. Compared to the independent variables of feed and gas flow rates shown in Table 3-5, inlet temperature had the least influence on the general outcomes, as it was only significant when optimizing the outcome of the ED. Thus, the inlet temperature at the low limit was fixed for general optimization. A design space (**Fig. 3-10**) showing the optimized process parameters was plotted by assembling the desired parameter combinations obtained from Fig. 3-5a to Fig. 3-8a. The arrows on the figure indicate the location of the parameter combination that met the targets. Different colors indicate the number of targets met in total within the parameter combination range. The parameter combination range meeting all four targets, which is marked in red, reflected the optimal region for preparing high-quality DPI formulation particles.

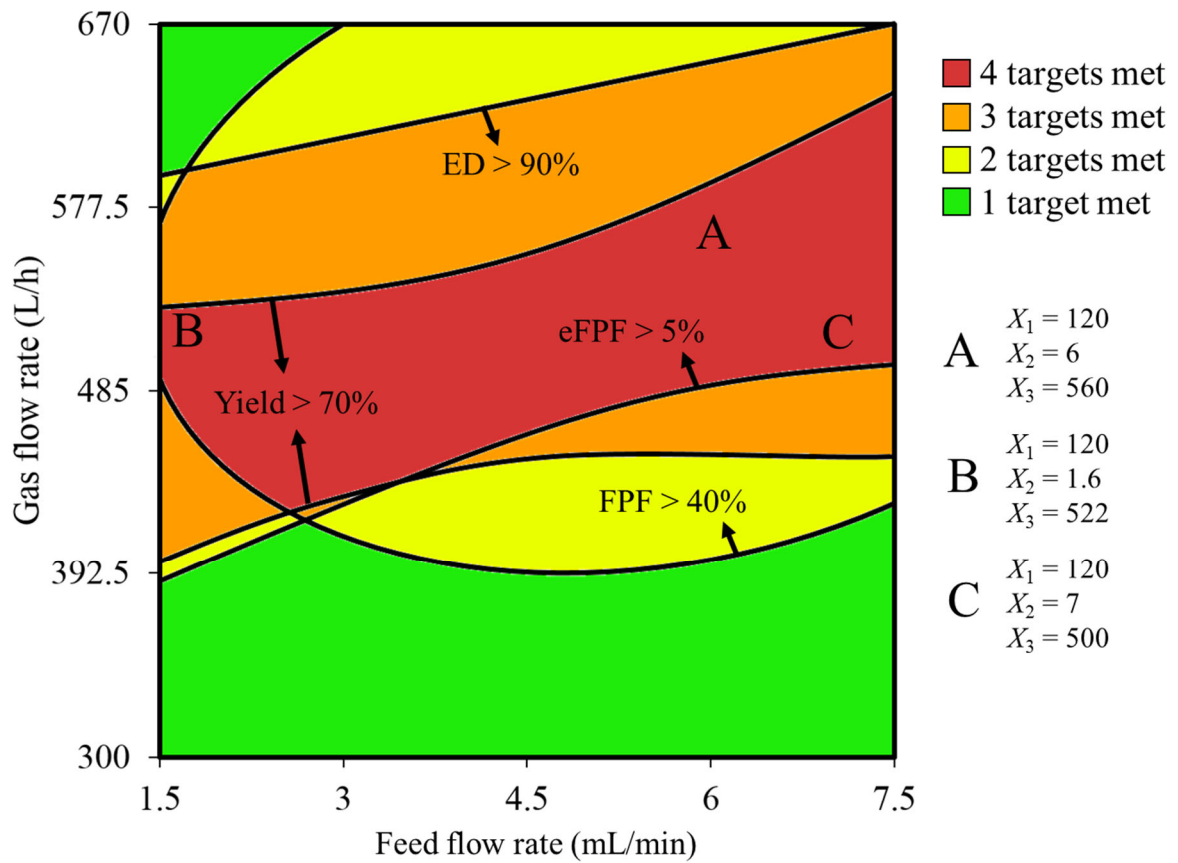


Fig. 3-10 The predicted design space for levofloxacin/phytoglycogen/leucine spray-dried particles. The inlet temperature was fixed at 120°C. Three process parameter combinations marked as A, B, and C were chosen from the red “four targets met” zone and were evaluated to validate the credibility of the design space. (X_1 = inlet temperature, X_2 = feed flow rate, and X_3 = gas flow rate)

3.2.5 Properties of the optimized runs

The area meeting all targets indicated the most desirable combination of process parameters. Three points, A (X_1 , 120°C; X_2 , 6 mL/min; X_3 , 560 L/h), B (X_1 , 120°C; X_2 , 1.6 mL/min; X_3 , 522 L/h), and C (X_1 , 120°C; X_2 , 7 mL/min; X_3 , 500 L/h), were selected from the optimized region meeting all four targets in the design space. To validate the credibility of the design space, the inhalation performance, and the percentage yield of the products prepared with the chosen parameter combinations were evaluated. The experimental results were anticipated to meet the 95% prediction interval derived from the predicted values. The predicted and experimental values of properties of the optimized particles are shown in **Table 3-6**. Among 12 outcomes values, 11 were within the 95% prediction interval range, indicating that the properties of particles prepared by optimized spray-drying conditions were well predicted.

Table 3-6 Predicted and experimental values of optimized runs A, B, and C in each response. Asterisk represents the experimental value within the 95% prediction interval. The predicted values of responses were calculated using the Unscrambler® X software. (X_1 = inlet temperature, X_2 = feed flow rate, X_3 = gas flow rate)

Optimized run		Response			
		Emitted dose (Y_1 ,%)	Fine particle fraction (Y_2 , %)	Extra-fine particle fraction (Y_3 , %)	Percentage yield (Y_4 , %)
A $X_1 = 120^\circ\text{C}$ $X_2 = 6 \text{ mL/min}$ $X_3 = 560 \text{ L/h}$	Predicted	96.05	52.90	6.08	72.02
	Experimental	93.50*	47.38*	7.28*	68.97*
	Difference	-2.55	-5.52	+1.2	-3.05
	95% Interval	91.05–101.05	40.23–65.57	3.48–8.68	61.15–82.89
B $X_1 = 120^\circ\text{C}$ $X_2 = 1.6 \text{ mL/min}$ $X_3 = 522 \text{ L/h}$	Predicted	95.48	41.01	7.66	70.32
	Experimental	90.22	39.25*	8.05*	64.03*
	Difference	-5.26	-1.76	+0.39	-6.29
	95% Interval	90.48–100.48	28.34–53.68	5.06–10.26	59.45–81.19
C $X_1 = 120^\circ\text{C}$ $X_2 = 7 \text{ mL/min}$ $X_3 = 500 \text{ L/h}$	Predicted	98.48	49.76	5.21	73.99
	Experimental	94.50*	44.92*	7.50*	68.00*
	Difference	-3.98	-4.84	+2.29	-5.99
	95% Interval	93.48–103.48	37.09–62.43	2.61–7.81	63.12–84.86

SEM images of particles, which were prepared using the optimized spray-drying parameters, are shown in

Fig. 3-11. Particle batches A and C shared similarities in shape, which were round and spherical. Conversely, batch B particles, which were prepared with a feed flow rate at a low level, exhibited a less spherical and rough nature.

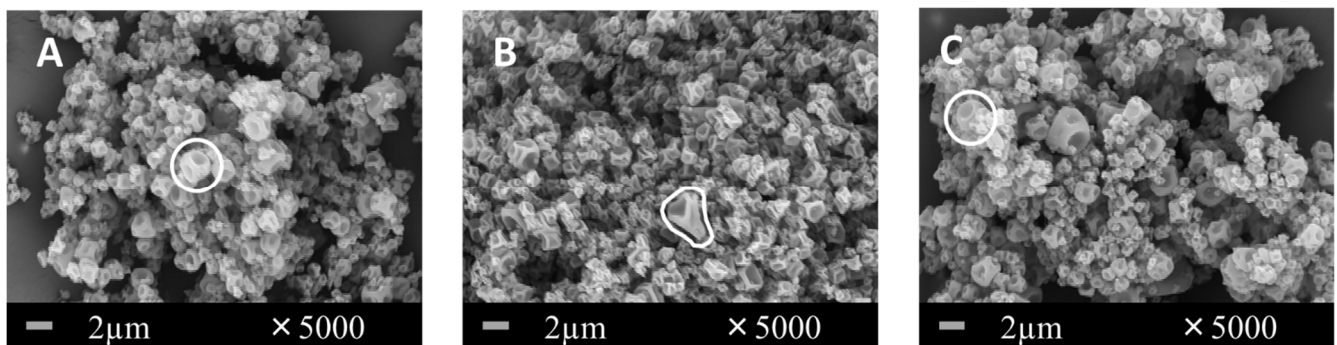


Fig. 3-11 SEM micrographs of the three optimized formulations A, B, and C. The corresponding process parameter combination of the spray-drying runs is shown in Fig. 3-10. The indicator shows a plump particle in batches A and C. Comparatively, the indicated particle in validation run B exhibits less spherical and rough shape.

The deposited percentages on ACI stages of the optimized formulations A, B, and C are shown in **Fig. 3-12**.

Although their general deposition behaviors share similarities, the optimized run C had more particles deposited on stage 5 rather than on stage 7, which is different from the other two batches.

The SDPs for checking the validity of optimization results for rifampicin using the optimized parameter combination A ($X_1 = 120^\circ\text{C}$, $X_2 = 6 \text{ mL/min}$, $X_3 = 560 \text{ L/h}$) was additionally prepared. The outcomes of the powder batch are shown in **Table 3-7**. The experimental values in each response met all four target values.

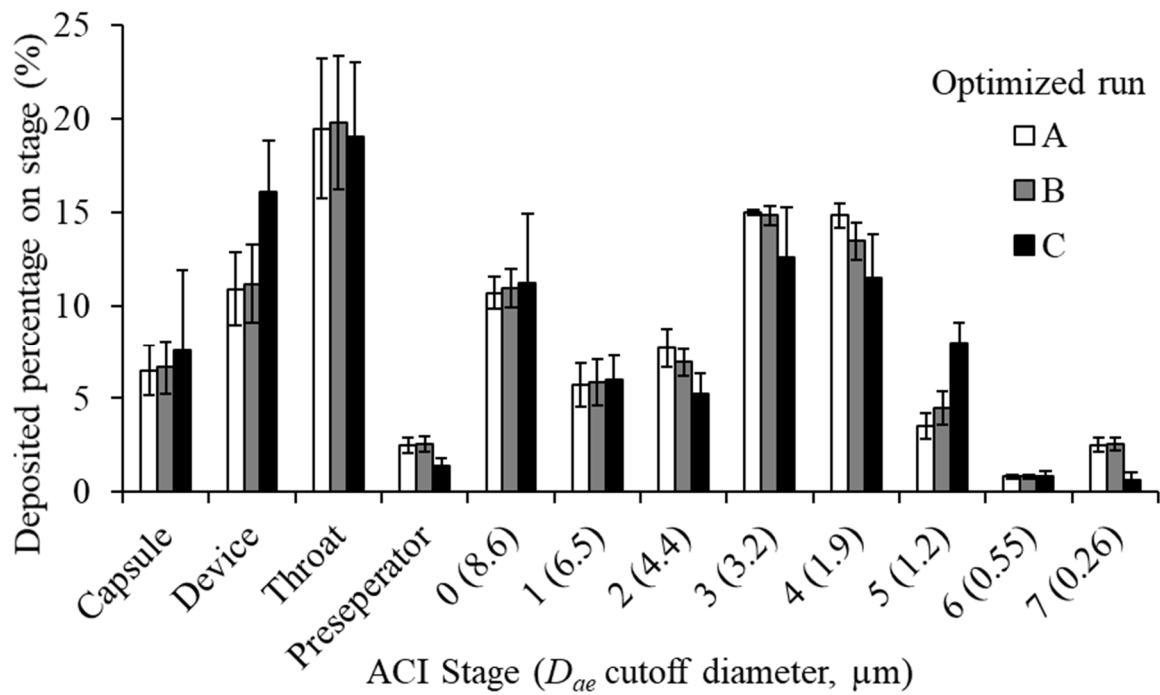


Fig. 3-12 Deposited percentage of the optimized runs A, B, and C on stages of an ACI using a 60 ± 5 L/min air flow rate for a 5 s inhalation. Values are represented as mean \pm SD ($n = 3$).

Table 3-7 Target and experimental values of the rifampicin/phytglycogen/leucine formulations in each response.

Response	Target value	Experimental value
Emitted dose (%)	90	99.65
Fine particle fraction (%)	40	40.08
Extra-fine particle fraction (%)	5	6.16
Percentage yield (%)	70	74.33

3.3 Discussion

3.3.1 Behavior of the additives

Other than PyG, the amino acid, LEU, was also selected to be the spray-drying additive. PyG formed aggregates due to the presence of the poor solvent ethanol, concerning its hydrophilic property. The mixture of ethanol and water was chosen is due to an enhancement of the evaporation rate of spray-drying precursor droplets. If the solvent contains 100% of water, the droplets will be hard to evaporate and remain in a liquid state on the wall of the drying tower of the spray-dryer. This phenomenon may lead to a bad influence on product yield as solid content remaining on the tower wall is no longer collectible. On the other hand, if the ethanol content in the spray-drying precursor increases (for example to 50% volume ratio), the hydrophilic drug LVFX would no longer be soluble, resulting in an uneven drug loading of SDPs.

Regarding Fig. 2-2, the SDPs of LVFX have sphere, needle, and other irregular shapes, which are not favorable in terms of uniformity. After the addition of PyG into the formulation, the major morphological property of the powders was taken over by PyG. Deflated ball shapes of the SDPs shown in Fig. 2-2c were derived from the spray-dried PyG. Concerning the molecular size and hydrophilicity of PyG and LVFX, LVFX may be incorporated into the PyG matrix and thus interfering with the particle morphology.

Different from the findings in Chapter 1, the SDPs of PyG did not exhibit porous particles, even the spray-drying precursor consist of a 20% ethanol volume ratio. The difference is attributed to the contrasting properties of the APIs, RFP in Chapter 1, and LVFX in Chapter 2. As mentioned in Section 2.3.3, porous particles may relate to the

solute diffusion⁸¹. RFP has a bigger molecular size and higher solubility in ethanol than LVFX. Concerning a lower diffusion coefficient, RFP may move slowly towards the droplet center because of high molecular size during the solvent evaporation process of an atomized precursor droplet. Moreover, as ethanol has a lower boiling point than water, the ethanol phase will primarily evaporate in the drying chamber. Since RFP has a high solubility in ethanol, the RFP molecules may solidify faster than PyG. Considering the phytoglycogen in precursor is evenly dispersed, the particles may have higher chances to become porous. In the case of LVFX, it has similar hydrophilicity to PyG, therefore the lag of solidification time between them may be shorter, resulting in the production of non-porous hollow particles.

3.3.2 Credibility of the design model

The properties of final products obtained by the spray-drying method are highly influenced by the parameters, especially inlet temperature, feed flow rate, and gas flow rate^{88,92-95}. Therefore, enhancement of the deep lung delivery of SDPs of LVFX/PyG/LEU was aimed by optimizing these three spray-drying process parameters using RSM. The final particles were anticipated to meet the required standard in four outcomes: ED, FPF, eFPF, and percentage yield. ED, FPF, and eFPF served as references for the inhalation performance of powders. The percentage yield of particles can represent an indicator of the economic effectiveness of the preparation process.

Low *p*-values (< 0.05) were obtained in each model of responses, indicating that the null hypothesis could be rejected, and the models were expected to be meaningful. Moreover, a lack of fit F-test for ANOVA was performed to determine the degree of errors that existed within the prediction. The *p*-values obtained for the lack of fit in each outcome were higher than 0.05, indicating the absence of a lack of fit within the model. To assure model credibility,

the values of R^2 , adjusted R^2 , and predicted R^2 were determined. Although an R^2 value above 0.8 indicates that the data are close to the fitted regression line, it cannot determine whether the estimated terms are biased, since the R^2 will be higher in the presence of more predictors. Therefore, the adjusted and predicted R^2 values are required to determine the reliability of a model. An adjusted R^2 is a modified R^2 in terms of the number of predictors in the model. The predicted R^2 represents the ability of a regression model to predict the responses for new observations. These two values can be negative and are always lower than R^2 . All adjusted R^2 values remain higher than 0.8 except for that of FPF. According to this data, the model of ED, eFPF, percentage yield, and aerodynamic diameter were not over-specified, and the model of FPF may be over-specified. Except for the model of aerodynamic diameter, all predicted R^2 values were lower than that of the R^2 to some extent (0.3270–0.4879), suggesting the presence of random ‘noise’ within those results possible because of excessive predictors in the model. Compared with other models, the model predicting aerodynamic diameter achieved the highest predicted R^2 value, at 0.8501, indicating that the regression model has a better ability to predict the responses for new observations.

The predicted versus reference scatter plot (Fig. 3-4) indicates that the data were better modeled if the slopes were close to 1. A bias value close to zero indicates a random distribution of points about the regression line. However, as the RMSED and SED of all responses were close, the biases were insignificant. This result also indicated that the data is a good fit for the model.

The importance of linear, quadratic, and interaction terms in the model was evaluated by p -values, as shown in Table 3-4. Except for β_0 , only terms with β -coefficients that have p -values lower than 0.05 were included in the

equation. ED had the most included terms in the equation, indicating that the response was influenced by the most variables (Eq. 3-1). Three terms were also introduced in the equation for FPF (Eq. 3-2). Both equations for percentage yield and aerodynamic diameter included two terms that reject the null hypothesis (Eqs. 3-4&5). The equation for eFPF only included the linear term for the gas flow rate (Eq. 3-3).

3.3.3 Relationship between independent and response variables

Particle properties were evaluated to determine the influence of experimental variables. Figs. 3-5a&b show that the gas flow rate was the most important for ED. The two figures indicated that a high gas flow rate will result in a low ED. Indeed, the gas flow rate determined the atomization force being introduced on a droplet⁹⁹. By enduring a high degree of atomization force, the droplet will fragment into small pieces. After drying, these pieces would form small particles. Additionally, the degree of ED was strongly associated with the static charge contained in the capsule, since this will interfere with the normal release of particles from the capsule¹⁶. In this case, particles with smaller sizes originating from small droplets atomized by a high gas flow rate would have a high chance of being trapped by static charges. Fig. 3-5b shows that the higher ED was obtained at the two extremes of temperature. A high inlet temperature favors a decrease in particle density⁹⁴. A decreased particle density may be beneficial to be mobilized by the inhalation airflow. Besides, when the temperature is at the low extreme, the particles become denser and aggregation of particles would be hindered, also leading to a result of high ED. In the case of a high gas flow rate, small particles are more fragile to agglomeration. As particles with low density at 180°C or particles with relatively high water content at 120°C are easier to agglomerate, the ED would be favorable at about 150°C. Fig. 3-5c shows that both inlet temperature and

feed flow rate had no significant influence on the ED when the gas flow rate was fixed at 300 L/h since the difference between the red and the blue regions was less than 5%, compared to the ~12% difference exhibited in Fig. 3-5a&b.

The optimal range for the two experimental parameters for a high level of FPF appeared as an oval-shaped region (Fig. 3-6a). When the inlet temperature was fixed at 120°C, the feed flow rate should be fixed at 3–7.5 mL/min, and the gas flow rate should be fixed at 485–670 L/h. Most particles prepared in that combination could be delivered into stage 2 or lower of ACI. As a high gas flow rate represents a strong atomization force, particles with smaller sizes would be more likely to form. A lower geometric median particle diameter reduced the product with the square-rooted value of particle density, leading to the reduced aerodynamic particle diameter (Eq. 1-1). It would be beneficial to achieve a higher FPF if the aerodynamic particle diameter could be reduced to $< 5 \mu\text{m}$. A higher feed flow rate may produce more solvent vapor inside the chamber, thus lowering the drying rate of droplets by reducing the exhaust temperature¹⁰⁰. A higher level of moisture would affect the size of particles by reducing the drying efficiency, possibly resulting in a low FPF¹⁰¹. Fig. 3-6b also indicated that a high gas flow rate was essential for obtaining a high FPF. When the gas flow rate is fixed at the high limit, the feed flow rate should be high, and the inlet temperature should be low in order to fabricate finer particles (Fig. 3-6c). The gas flow rate is the most critical factor to determine the particle size due to the impact of the atomization force on feed droplet size. Higher content of solvent vapor may lower the outlet temperature, leading to an effective heat transfer to dry the feed droplets. The drying rate would be the lowest when the inlet temperature is at the low limit. The feed droplets have more drying time to form a smooth surface at a low drying rate; the extended time also allows water content inside the particle easier to escape and evaporate. A smooth surface

had a low air resistance compared to a rough surface; lower water content may lead to a change of particle size and finally affect the FPF. Contrarily, a high drying rate may lead to the formation of a large shell on the droplet surface. Although an evaporating droplet with a large shell may end up as a hollow particle with low density, the large particle size may hinder its final FPF.

A higher proportion of extra-fine particles were targeted in order to deliver the materials deeper into the alveoli. Figs. 3-7a&b indicated that a higher gas flow rate, i.e. stronger atomization force, was helpful for preparing particles on an extra-fine scale. Figs. 3-7a&c show that a lower feed flow rate might facilitate the formation of extra-fine particles. During the spray-drying process, the collision between droplets will occur. There are three possible outcomes after a droplet collision: coalescence, fragmentation, and bounce^{102,103}. The velocity of atomized droplets may decrease due to a low feed flow rate. If the impact force is not sufficient to break the surface tension of droplets, the colliding droplets would bounce against each other to prevent coalescence, hence the droplet size would remain the same instead of enlargement¹⁰⁴. No significant impact of inlet temperature on the extra-fine particle fraction was observed. Furthermore, the difference between the blue region and the red region in Fig. 3-7c was only around 2.3%, indicating that the feed flow rate and inlet temperature had a minor effect on the preparation of extra-fine particles.

Figs 3-6&7 indicated that a high gas flow rate was beneficial for both FPF and eFPF. However, the parameter combination range for optimal responses differed. By fixing the inlet temperature at a low limit, a feed flow rate at the middle level to the high limit facilitated the fabrication of overall fine particles. Yet, a low feed flow rate promoted the eFPF value to the greatest extent. The change of aerodynamic particle size distribution has a major contribution to this

phenomenon. Spray-drying run 5 has low FPF (34.8%) but high eFPF (9.6%); comparatively, spray-drying run 7 has high FPF (50.2%) but lower eFPF (6.4%). For Formulation 5, although the fraction of particles that can enter stage 2 or deeper is low, a relatively high fraction of particles is deposited on stage 5 (**Fig. 3-13**). More particles could be inhaled into stage 2 or deeper; however, the deposited percentage on stages 5 to 7 is relatively low, as shown in the result of Formulation 7. The change of aerodynamic particle size distribution is heavily responsible in this situation. Based on the desired destination of various drugs within the lung, this difference could be beneficial. When using drugs to treat asthma or other diseases involving the trachea, a feed flow rate at the middle level to the high limit could be effective for preparing a higher proportion of fine particles. Conversely, to treat pneumonia by LVFX, a low feed flow rate would be better to achieve a high eFPF value.

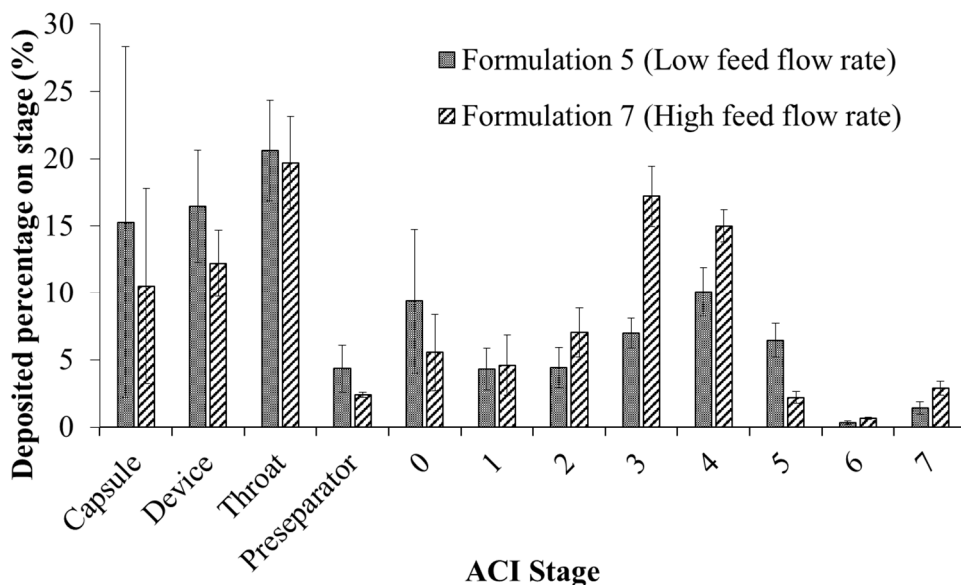


Fig. 3-13 The deposited percentage on ACI of formulation 5 and 7 at a flow rate of 60 ± 5 L/min for 5 s. Values are represented as mean \pm SD (n = 3).

Apart from the inhalation performance of particles, the percentage yield, which is an indicator of economic effectiveness, was also included in the RSM optimization design. As shown in Figs. 3-8a&b, a high percentage yield was obtained when the rate of gas flow was around the middle level. A high gas flow rate might not be suitable for obtaining a higher yield, owing to the formation of small particles with insufficient density. Those particles would be delivered to the filter of the spray-dryer rather than to the collection bottle. If the gas flow rate was low, the particles might remain in the cyclone separator and fail to drop into the collection bottle, owing to the weak air pressure. Both feed flow rate and inlet temperature exerted minor effects on percentage yield (Figs. 3-8a&b). However, an oval blue region is shown in Fig. 3-8c when the gas flow rate was fixed at 670 L/h. Both parameters affected the percentage yield. A high feed flow rate and a high or low inlet temperature were significant in terms of a high percentage yield. Increasing the feed flow rate would increase the solid content in the drying chamber. Droplet collision would also be more likely to occur, resulting in coarser products. Both high and low inlet temperatures can also enhance the percentage yield. At low inlet temperature, denser particles could form under a slow drying rate⁹⁴. However, if a high inlet temperature was used, the particle structures may form earlier without shrinkage under a high drying rate and therefore, a high percentage yield could be obtained.

Unlike other responses, a target value was not set for aerodynamic particle diameter since there were limitations with particles that had excessively high or low aerodynamic diameters. For example, it is difficult to deliver particles with a high aerodynamic diameter deep into the lung^{11,21}. Meanwhile, it is easier to trap particles with a low aerodynamic diameter based on static charges. As shown in Fig. 3-9, the gas flow rate had a strong influence on the

diameter of aerodynamic particles. This finding is consistent with the predicted models of ED, FPF, and eFPF. Particles fabricated under a high gas flow rate are more likely to have a low aerodynamic diameter, leading to a low ED, a high FPF, and a high eFPF.

3.3.4 Effectiveness of the design space

A 2D design space for the optimization of particle preparation is shown in Fig. 3-10. Since the influence of inlet temperature on the responses was essential at the low limit, inlet temperature at the low limit was selected as a fixed parameter in the design space. The red region was able to fulfill the four targets of ED above 90%, FPF above 40%, eFPF above 5%, and percentage yield above 70%, within a 95% prediction interval. Although a gas flow rate at the high limit is advantageous for preparing fine particles, it is not favorable for preventing static charges that can interfere with the release of particles, thus not economically efficient (percentage yield < 70%)¹⁶. Therefore, the optimized range of the gas flow rate parameter mostly fell around the middle level. As long as the gas flow rate parameter was at the middle level, favorable product outcomes could be obtained at all levels of the feed flow rate. To determine the credibility of the design space, products that were prepared using the three sets of process parameters within the red region were evaluated. As shown in Table 3-6, most responses fell within the 95% prediction interval. The only response that did not meet this requirement was the ED of batch B, which was lower than the predicted response, at 5.26%. In the evaluation test, 11 out of 12 responses fell within the prediction interval, showing that the design space was generally trustworthy; the response values were well predicted. The morphology of the three optimized runs is also shown in Fig. 3-11. The feed flow rate for preparing particles of batch B was lower than that for

batches A and C, resulting in less spherical and rough particle shapes. Under the same atomization condition, the feed flow rate may have a positive relationship with the droplet size. The atomization force would be shared by more feed suspension in the nozzle tip with an increased feed flow rate, leading to a larger droplet size after atomization. During the experimental process, the outlet temperature of the spray-dryer is $< 50^{\circ}\text{C}$ at a feed flow rate of 6 mL/min. Alternately, the outlet temperature will become high ($> 55^{\circ}\text{C}$) if the feed flow rate is at 1.6 mL/min. Hence, the temperature gradient is higher when the feed flow rate is higher. This phenomenon may be due to a decrease in vaporization heat originating from the liquid content of droplets. Concerning a higher temperature gradient, the drying chamber may have a higher drying rate. Moreover, the size of the droplets may play a role in the drying process, taking its surface area into account which contacts the hot air to receive heat energy. Shrinkage of particles would occur apparently in larger particles, as diffusion of solid contents from the outer surface towards the inner part of droplets was more difficult, due to the larger volume of solvent in a single droplet⁶⁴. As shown in Table 3-7, the lowest FPF was found from batch B particles, which was also consistent with the 95% prediction interval. From the result in Fig. 3-12, the deposited percentage on stage 5 from batch C particles was higher than those from batches A and B, while the percentage on stage 7 was less. This phenomenon may be due to the lowest gas flow rate of batch C among the optimized runs, leading to a lower aerodynamic particle diameter compared to particles from batches A and B. However, all batches of particles still share a similar value in eFPF, since extra-fine particles include those with $< 1\ \mu\text{m}$ aerodynamic diameter, which are deposited on stages 5 (diameter range: $0.55 - 1.2\ \mu\text{m}$), 6 ($0.26 - 0.55\ \mu\text{m}$), and 7 ($< 0.26\ \mu\text{m}$).

The validity of the design space for another drug was evaluated with rifampicin. As shown in Table 3-7, the

powders showed the ability to fulfill the targets, with excellent ED and eFPF (> 10% markup compared to the target value). Herein, the usefulness of the design space in another drug is demonstrated. The exploration of the potential of the design space is still working in progress; it is useful in preparing good inhaler formulations of general validity, hence making contributions in the field of pulmonary delivered drug formulations.

3.4 Summary

LVFX-containing particles with fair alveolar delivery properties were successfully fabricated by optimizing the selected spray-drying parameters of inlet temperature, feed flow rate, and gas flow rate. RSM was adopted as a statistical tool to perform the optimization process. Seventeen spray-drying runs were conducted regarding the face-centered central composite design. The ED, FPF, eFPF, percentage yield, and aerodynamic particle diameter of products were evaluated. A design space introducing the optimized independent variables was plotted by compiling the response surfaces. Optimized runs in the design space were also evaluated to validate the credibility of the design space, and 11 of 12 responses were within the 95% prediction interval of the predicted values. The morphology of the desired particle was assessed and taken as a reference for high-quality DPI formulation powders. Concerning the influence of process parameters, the most critical parameter was the gas flow rate, owing to its significant contribution ($p < 0.05$) on droplet size.

Chapter 4 Conclusions

Herein, the design of PyG-based DPI formulations was performed. In Chapter 1, the morphology of SDPs using PyG as excipient was successfully controlled by manipulating the precursor property. Interestingly, large-wrinkled particles can deliver drugs effectively to peripheral lungs compared to porous particles. The safety of PyG was verified by *in vitro* cytotoxicity tests using pulmonary cell lines. The effects of PyG as a functional additive on the expression of pro-inflammatory cytokine genes and phagocytosis in RAW264.7 cells were also confirmed. The innovative carrier particles proposed in this chapter for efficient alveolar delivery are anticipated to improve the design of future formulations. Nevertheless, further investigation on the electroconductivity and the solvent composition of the novel carrier-based formulation for efficient alveolar delivery is warranted. In Chapter 2, an optimization of the process parameters using DoE was performed for the design of PyG-based DPI formulations with enhanced deep lung delivery ability and economic efficiency. The most influencing process variables corresponding to each property of the products were investigated. The performance and validity of the optimization design were also ensured. Concerning diseases that are related to unhealthy peripheral airways, drug formulations with extra-fine properties achieved by the PyG-based particles may be useful to perform target site delivery.

Up to the present, the options of DPI additives are still very limited. Because of the numerous advantages and interesting phenomenon, macromolecular polysaccharides like PyG are worth investigating and developing as one of the mostly-used additives to prepare DPI formulations. PyG-based particles provide flexible morphology, size, and inhalation performance. The target region of the inhalable API to deposit could be technologically tailored. The

promising approach of using DoE for optimizing the process parameters to design PyG-based formulations was also demonstrated. The author believes the findings on PyG as a spray-drying additive can contribute to the development of pulmonary delivery formulations by providing reliable designs.

Chapter 5 Experimental section

5.1 Experimental section of Chapter 2

5.1.1 Materials

PyG (MW 10^6 – 10^7) was provided by Kewpie Corp. (Tokyo, Japan). RFP (MW 822.94) was supplied by Kaken Pharmaceutical Co. Ltd. (Tokyo, Japan). Acetonitrile was purchased from Fujifilm Wako Pure Chemical Corp. (Osaka, Japan). Ethanol was supplied by Japan Alcohol Trading Company Ltd. (Tokyo, Japan). All organic solvents were of reagent grade. Deionized water was purified by the Milli-Q system (Merck).

5.1.2 Cell culture

Human lung carcinoma A549 cells and murine macrophage-like RAW264.7 cells were cultured by standard methods in Dulbecco's modified Eagle medium (Nacalai Tesque, Kyoto, Japan). Human lung carcinoma Calu-3 cells were cultured in Eagle's minimal essential medium (ATCC, Manassas, VA, USA). Both media contained 10% (v/v) fetal bovine serum (Biosera, MO, USA) and 0.1% (w/v) penicillin-streptomycin solution (100 U/mL and 100 μ g/mL, respectively; Nacalai Tesque). All cells were cultured at 37°C in a humidified 5% CO₂ incubator.

5.1.3 Tetrazolium salt WST-8 cell viability test

The cell viability was determined using a Cell Counting Kit-8 (CCK-8; Dojindo Molecular Technologies, Kumamoto, Japan). A549, Calu-3, and RAW264.7 cells were seeded at 1×10^4 cells/well in 96-well plates (Thermo Fisher Scientific, Waltham, MA, USA), and cultured for 24 h, followed by were exposed to various concentrations of PyG for 24 h. The absorbance values were measured at a wavelength of 450 nm 2 h after adding CCK-8 reagent diluted to 1/20 with culture medium. The cell viability (%) was calculated using the following equation:

$$\text{Cell viability (\%)} = \frac{\text{Absorbance}_{\text{sample}}}{\text{Absorbance}_{\text{control}}} \times 100\%$$

Eq. 5-1-1

Absorbance_{sample} denotes the absorbance value of a well-treated with a sample solution, whereas Absorbance_{control} represents that of the well treated with culture medium only.

5.1.4 Quantitative PCR

RAW264.7 cells were exposed to various concentrations of PyG for 24 h. Total RNA was extracted with ISOGEN II (Nippon Gene, Tokyo, Japan) and used for first-strand cDNA synthesis with ReverTra Ace qPCR RT Master Mix (Toyobo, Osaka, Japan) according to the manufacturer's protocols. The expression levels of pro-inflammatory cytokine genes were measured using a LightCycler 96 System (Roche Diagnostics, Mannheim, Germany) and Power SYBR Green Master Mix (Thermo Fisher Scientific). Gene-specific primers of IL-1 β , inducible nitric oxide synthase (iNOS), TNF- α , and glyceraldehyde-3-phosphate dehydrogenase (GADPH) were designed as shown in **Table 5-1-1**. The expression level of each target gene was calculated using the $2^{-\Delta\Delta C_t}$ method and normalized to that of GAPDH as the reference gene.

Table 5-1-1 Gene-specific primers used in quantitative PCR

Genes	Primer sequences	
	Forward	Reverse
IL-1 β	5'-TGAGCACCTTCTTTCCTTCA-3'	5'-TTGTCTAATGGGAACGTCACAC-3'
iNOS	5'-CTTTGCCACGGACGAGAC-3'	5'-TCATTGTACTCTGAGGGCTGAC-3'
TNF- α	5'-TCTTCTCATTCCCTGCTTGTGG-3'	5'-GGTCTGGGCCATAGAACTGA-3'
GADPH	5'-GGAAAGCTGTGGCGTGATG-3'	5'-CCAGTGAGCTTCCCGTTCAG-3'

5.1.5 Uptake of polystyrene latex beads by macrophage-like cells

RAW264.7 cells were seeded at a density of 5×10^4 cells in a 96-well black plate and incubated for 12 h. The cells were exposed to various concentrations of PyG for 24 h. The cells were incubated with 0.5% (w/v) fluorescent polystyrene latex beads (1 μm diameter, yellow-green-labeled, #L4655; Sigma) for 1 h. The latex beads were washed three times with Hanks' balanced salt solution. The nucleus was also stained with Hoechst 33342 (1 $\mu\text{g}/\text{mL}$; Sigma) for 0.5 h. The fluorescence intensity was measured by using an EnSpire 2300 Multimode Plate Reader (PerkinElmer, Waltham, MA, USA). A confocal laser scanning microscope (LSM700, Carl Zeiss, Oberkochen, Germany) was used to observe the cellular uptake of fluorescent latex beads.

5.1.6 Particle diameter analysis

The particle diameter of PyG in water and ethanol solutions was evaluated by DLS using a Microtrac UPA (MicrotracBEL Corp., Osaka, Japan). The water/ethanol ratio of the solvent varied from 100/0 to 50/50 (v/v). The detection range of the analyzer is 0.003–6 μm . The measurement time was fixed at 1 min. The equivalent volume

diameters at 10%, 50%, and 90% cumulative volume (D_{10} , D_{50} , and D_{90} , respectively) were measured using a published method¹⁰⁵.

5.1.7 Preparation of particles

Particles were fabricated from an RFP and PyG suspension by spray drying. The precursor was prepared by dropping ethanolic rifampicin solution into phytoglycogen solution using a peristaltic pump at a flow rate of 2 mL/min. The volume percentages of ethanol used were 10%, 20%, 30%, 40%, and 50%. The final solid concentration of RFP and PyG (1/5, w/w) in the precursor was 4 mg/mL. The spray-drying conditions were fixed in reference to a previous study⁴⁵. The inlet temperature was 130°C. The aspirator was set at the maximum percentage. The precursor was atomized through a 0.7-mm two-fluid nozzle by a spray dryer (B-290, Buchi K.K., Tokyo, Japan) at a feed rate of 5.5 mL/min. The drying gas (N₂/air) flow rate was 473 L/min. The percentage yield was calculated by the following equation:

$$\text{Percentage yield (\%)} = \frac{\text{Weight of spray dried particle product (mg)}}{\text{Weight of materials used (mg)}} \times 100\% \quad \text{Eq. 5-1-2}$$

RFP SDPs without PyG were additionally prepared using the same spray-drying conditions. The volume percentage of ethanol in the solvent was 30%. Moreover, RFP was also mixed with lactose DPI carrier (Inhalac® 230, MEGGLE Pharma, Germany) at a weight ratio of 1/67.5 to serve as a control group for *in vitro* aerosolization performance test.

5.1.8 Geometric particle size distribution analysis

Geometric particle size distribution was evaluated by laser diffraction using a particle analyzer under dry conditions (MT3300EXII; MicrotracBEL Corp.). The powder samples were dispersed in the air by an air jet at a pressure of 0.2 MPa. D_{10} , D_{50} , and D_{90} were evaluated. The span value is calculated by the following equation.

$$\text{Span} = \frac{D_{90} - D_{10}}{D_{50}}$$

Eq. 5-1-3

5.1.9 Scanning electron microscopy

Random images of SDPs were captured using a scanning electron microscope (Miniscope TM3030; Hitachi High-Technologies Corporation, Tokyo, Japan). Powder samples were set on a metal stub with double-sided adhesive carbon tape. The stub was coated with a thin layer of platinum under vacuum (E-1045, Hitachi Co., Ltd., Tokyo, Japan). The acceleration voltage was set as 15 kV.

5.1.10 Powder X-ray diffraction analysis

The crystallinity of powders was evaluated using the SmartLab X-ray diffractometer (Rigaku Co., Ltd., Tokyo, Japan). The powder samples were evenly distributed on a glass plate for detection. The scanning range and rate were 5–35° and 4°/min, respectively. The electric current and potential were 15 mA and 30 kV, respectively.

5.1.11 Differential scanning calorimetry analysis

Differential scanning calorimetry (DSC) was performed using the DSC-7000X instrument (Hitachi High-Tech Science Corporation; Tokyo, Japan). Each sample weighed between 3 and 5 mg was filled into crimped aluminum DSC pans. Indium was used as the calibration material. The purging nitrogen gas flowed at 50 mL/min. The pans were heated to 200°C at a rate of 10°C/min.

5.1.12 *In vitro* aerosolization performance of spray-dried particles

The aerosolization performance of particles was evaluated using an ACI (AN-200 system; Tokyo Dylec Corp., Tokyo, Japan). Powder samples (10 mg) were loaded into size 2 hydroxypropyl methylcellulose capsules (Qualicaps, Nara, Japan). The loaded capsule was installed in a Jethaler inhaler device (Tokico System Solutions, Ltd., Gunma, Japan). The collection plates for each stage were immersed in a 2% (v/v) solution of silicon in hexane to form a thin layer of silicon to reduce particle bounce. The drawing rate was set at 28.3 L/min, with the aspiration time adjusted for 4 L of airflow. The percentages of the drug recovered on each stage were determined using high-performance liquid chromatography (HPLC)^{106,107}. The inhalation parameters, namely, the emitted dose (ED), fine particle fraction (FPF), and extra-fine particle fraction (eFPF), were calculated for each formulation as follows:

$$\text{Emitted dose (ED) (\%)} = \frac{\text{Emitted dose (\mu g)}}{\text{Total recovered drug (\mu g)}} \times 100\% \quad \text{Eq. 5-1-4}$$

$$\text{Fine particle fraction (FPF) (\%)} = \frac{\text{Fine particle dose (\mu g)}}{\text{Emitted dose (\mu g)}} \times 100\% \quad \text{Eq. 5-1-5}$$

$$\text{Extra-fine particle fraction (eFPF) (\%)} = \frac{\text{Extra-fine particle dose (\mu g)}}{\text{Emitted dose (\mu g)}} \times 100\% \quad \text{Eq. 5-1-6}$$

The emitted dose is the difference between the quantity of the drug recovered from the entire setup and the remaining drug content in the capsule. The fine particle dose denotes the quantity of the drug recovered from stage 2 and below, and the extra-fine particle dose represents that from stage 5 and below.

5.1.13 HPLC analysis

The RFP concentration for loading capacity test and *in vitro* aerosolization performance test was analyzed by HPLC (e2695 and 2489; Waters, Milford, USA). The loading capacity of RFP was calculated by the following equation:

$$\text{Loading capacity (\%)} = \frac{\text{Drug content detected (\mu g)}}{\text{Predicted drug content (\mu g)}} \times 100\% \quad \text{Eq. 5-1-7}$$

A 4.6 × 250 mm YMC-ProC18 column (Inertsil ODS-2 5 μm; GL Sciences, Tokyo, Japan) was used at 40 °C. The injection volume and the detection wavelength were 10 μL and 240 nm, respectively. The mobile phase, water/acetonitrile/0.1% phosphoric acid (55/35/10, v/v/v), flowed at a rate of 1.0 mL/min¹⁰⁸. The retention time was approximately 5 min. The RFP content in a fixed weight of each formulation was also evaluated.

5.1.14 Statistical analysis

The results obtained from the cell viability, gene expression, and cellular uptake experiments were statistically analyzed. Comparisons between more than two groups were carried out using Tukey's *post hoc* test. The Pharmaco Basic software (Ver. 15; Scientist Press, Tokyo, Japan) was used for analysis. *P*-values < 0.05 indicated statistically significant differences.

5.2 Experimental section of Chapter 3

5.2.1 Materials

LVFX (Mw 370.38) was supplied by Ohara Pharmaceutical Co., Ltd. (Shiga, Japan). PyG was supplied by Kewpie Corporation (Tokyo, Japan). LEU (Mw 131.17) was purchased from Wako Pure Chemical Industries, Ltd. (Osaka, Japan). All other chemicals and solvents were of reagent grade.

5.2.2 Preparation of spray-dried particle samples

Prior to optimizing the process parameters of the spray-drying method, the solid composition ratio of the active pharmaceutical ingredient and additives was evaluated. The spray-drying conditions were as follows: inlet temperature, 120°C; feed flow rate, 4.5 mL/min; and gas flow rate, 485 L/h. The components of the suspension were prepared by dissolving materials (LVFX/PyG/LEU) into 240 mL of water; 60 mL of ethanol was added into the solute to obtain a 20/80 (v/v) ethanol/water suspension. The solid concentration of the suspension was 4 mg/mL. The ratio of LVFX/PyG/LEU was varied. The suspension was sprayed into droplets using a 0.7 mm two-fluid nozzle by a spray-dryer (B-290, Buchi K.K., Tokyo, Japan). Aspiration was set at 100%. Air supplied by a compressor was used as the drying and atomizing gas. The percentage yield was obtained by Eq. 5-1-2.

The spray-drying run for assessing the validity of optimization for another drug formulation was additionally prepared using the optimized parameters that are obtained subsequently. The feed composition was the same as above, while rifampicin was used instead of LVFX.

5.2.3 Preparation of jet-milled samples

LVFX was jet-milled with a Spiral Jet Mill AS (Hosokawa Micron Co., Osaka, Japan) to create particles of

reduced size. Particles were cracked under a grinding pressure of 0.5 MPa with nitrogen as an inert gas. Particles were fed to the grinding chamber and were collected in a filter bag.

5.2.4 Inhalation performance of dry powders

The preparation of the instrumental set-up was the same as Section 5.1.12. Following inhalation, the deposited powders in the capsule, the device, the pre-separator, the simulated throat, and on the stages were rinsed with 25 mL of phosphate buffer (pH 6.8). The LVFX content in the powders in each region was determined via HPLC (Section 5.2.8). The inhalation parameters (ED, FPF, and eFPF) were calculated based on the results of the HPLC analysis^{106,107}. The formulae used to calculate ED, FPF, and eFPF were Eq. 5-1-4 to Eq. 5-1-6, respectively.

5.2.5 Aerodynamic and geometric particle diameter of powders

The theoretical aerodynamic volume mean diameter (D_{ae}) was calculated by Eq. 1-1. The geometrical particle diameter for each sample was measured as mentioned in Section 5.1.8. The particle density was the quotient of the bulk density and true density of particles. To obtain the bulk density of particles, each powder sample (50 mg) was filled into a 5 mL measuring cylinder. The bulk density value is the quotient of the weight of the powder and the filled volume. The gas pycnometer (AccuPyc1330; Shimadzu Co., Ltd., Kyoto, Japan) was used to measure the true density of particles by loading the powders into the chamber. The experiments were performed in triplicates.

5.2.6 Face-centered central composite design – response surface methodology

Inlet temperature (X_1), feed flow rate (X_2), and gas flow rate (X_3) were selected as factors of the face-centered central composite model (Table 5-2-1). A sequence of designed experiments (17 runs in total) was conducted. Five response variables (Y_1 : ED, Y_2 : FPF, Y_3 : eFPF, Y_4 : percentage yield, and Y_5 : aerodynamic diameter) were included in

the analysis. A classical DoE analysis consisting of the Scheffe test and a multiple linear regression test was selected as the analytical method. The main effect interactions between two variables (X_1X_2 , X_1X_3 , X_2X_3) and quadratic terms (X_1^2 , X_2^2 , X_3^2) were considered in the calculations. The correlation between process variables and response variables could be summarized in the equation as follows.

$$Y_n = \beta_0 + \beta_1X_1 + \beta_2X_2 + \beta_3X_3 + \beta_{1,2}X_1X_2 + \beta_{1,3}X_1X_3 + \beta_{2,3}X_2X_3 + \beta_{1,1}X_1^2 + \beta_{2,2}X_2^2 + \beta_{3,3}X_3^2 \quad \text{Eq. 5-2-1}$$

where Y denotes the response variable, X represents the independent variables, β_0 is the value at the center point (0,0,0) of the design, β represents the regression coefficients computed from the experimental values of Y, and X_aX_b (a and b = either 1, 2, or 3) denotes the interaction terms. The calculation was performed by the Unscrambler® X Ver. 10.1 (CAMO software Japan, Tokyo, Japan).

Table 5-2-1 Values of process variables.

Process variable	Low limit (-1)	Central (0)	High limit (1)	Unit
Inlet temperature (X_1)	120	150	180	°C
Feed flow rate (X_2)	1.5	4.5	7.5	mL/min
Gas flow rate (X_3)	300	485	670	L/h

5.2.7 Scanning electron microscopy

Micrographs were obtained as demonstrated in Section 5.1.9.

5.2.8 HPLC analysis

The concentration of LVFX in the samples was quantified by HPLC (e2695 and 2489; Waters, Milford, USA).

A C_{18} reversed-phase column (COSMOSIL®, Nacalai Tesque Inc., Kyoto, Japan) was used. The mobile phase,

comprising 60% water and 40% methanol (pH = 3.0 adjusted by acetic acid), was maintained at a flow rate of 0.7 mL/min. The UV detection wavelength was 290 nm.

5.2.9 Statistical data analysis

Multivariate statistical analysis was conducted to optimize spray-drying conditions using classical DoE analysis, in which individual analyses of variance (ANOVAs) for each response were included. An R^2 value close to 1 represents a fair correlation between the predicted response value and the experimental response value. A p -value lower than 0.05 represents significance and indicates a good model. A p -value between 0.05 and 0.1 represents a marginal significance. A p -value higher than 0.1 indicates no significance.

Abbreviations

ACI	Andersen cascade impactor
ANOVA	Analyses of variance
API	Active pharmaceutical ingredient
CCK-8	Cell counting kit-8
DLS	Dynamic light scattering
DoE	Design of experiment
DPI	Dry powder inhaler
DSC	Differential scanning calorimetry
ED	Emitted dose
eFPF	Extra-fine particle fraction
EtOH	Ethanol
FPF	Fine particle fraction
GADPH	Glyceraldehyde 3-phosphate dehydrogenase
HPLC	High-performance liquid chromatography
IL	Interleukin
iNOS	Inducible nitric oxide synthase
LEU	L-leucine
LVFX	Levofloxacin hemihydrate
MW	Molecular weight
PCR	Polymerase chain reaction
PyG	Phytoglycogen
RFP	Rifampicin
RMSED	Root mean square error of deviation
RSM	Response surface methodology
SDP	Spray-dried particles
SD	Standard deviation
SED	Standard error of deviation
SEM	Scanning electron microscope
TLR	Toll-like receptor
TNF	Tumor necrosis factor

Acknowledgements

I would like to express my sincere gratitude to my supervisor and the vice-chair of my thesis committee Prof. Tozuka, Yuichi for his continuous support. His guidance and patience carried me through all the stages of writing my thesis. He is also my local guarantor who gave me the opportunity to complete my doctoral study in Japan. I would also like to acknowledge the chairman of my committee Prof. Doi, Mitsunobu who has been supportive in my thesis defense. His advice and suggestions made the thesis better. I am especially indebted to my mentor and the vice-chair of my thesis committee Prof. Kadota, Kazunori for his inestimable personal and professional guidance. He taught me a great deal about scientific research, career, and life in general. I am also grateful to Dr. Uchiyama, Hiromasa for his valuable comments and advice throughout my doctoral project. I also thank Prof. Fujimori, Ko and Dr. Koike, Atsushi for assisting the research with their knowledge in biology. My sincere thanks also go to Prof. Yang, Zhijun, my former supervisor at Hong Kong Baptist University.

This thesis would not be possible without the support of many current and former colleagues: Dr. Fujimori, Miki; Nogami, Satoshi; Yamashita Rikiya; Takeo, Tomo; Tachikawa, Tomoko; Yukimoto, Atsushi; Hatanaka, Yuta; Imakubo, Tetsuya; Yamano, Chika; and Irifune, Minako.

I am grateful to Osaka Medical and Pharmaceutical University (formerly Osaka University of Pharmaceutical Science) for all assistance and support that allowed me to focus my efforts and attention on my project.

I want to extend my thanks to all companies that have supported the project. Kewpie Corp. (Tokyo, Japan) has provided phytoglycogen, the macromolecular polysaccharide. Quality Design Co., Ltd. (Kyoto, Japan) has provided professional advice on experimental design analysis. Tokico System Solutions, Ltd. (Kanagawa, Japan) has lent the Jethaler® device. MicrotracBEL Corp. (Osaka, Japan) has lent the MT3300EXII for particle size analysis.

Nobody has been more important to me in the pursuit of this project than the members of my family. I wholeheartedly appreciate my parents Veronica and Andrew; my sister Emily; my brother Andre; and my aunt Hody for their invaluable support.

This research was supported by the Hosokawa Powder Technology Foundation (Osaka, Japan).

References

- (1) Weers, J. G.; Miller, D. P. Formulation Design of Dry Powders for Inhalation. *J. Pharm. Sci.* **2015**, *104* (10), 3259–3288. <https://doi.org/10.1002/jps.24574>.
- (2) Sou, T.; Orlando, L.; McIntosh, M. P.; Kaminskas, L. M.; Morton, D. A. V. Investigating the Interactions of Amino Acid Components on a Mannitol-Based Spray-Dried Powder Formulation for Pulmonary Delivery: A Design of Experiment Approach. *Int. J. Pharm.* **2011**, *421* (2), 220–229. <https://doi.org/10.1016/j.ijpharm.2011.09.018>.
- (3) Pilcer, G.; Amighi, K. Formulation Strategy and Use of Excipients in Pulmonary Drug Delivery. *Int. J. Pharm.* **2010**, *392* (1–2), 1–19. <https://doi.org/10.1016/j.ijpharm.2010.03.017>.
- (4) Labiris, N. R.; Dolovich, M. B. Pulmonary Drug Delivery. Part I: Physiological Factors Affecting Therapeutic Effectiveness of Aerosolized Medications. *Br. J. Clin. Pharmacol.* **2003**, *56* (6), 588–599. <https://doi.org/10.1046/j.1365-2125.2003.01892.x>.
- (5) Sakagami, M. In Vivo, in Vitro and Ex Vivo Models to Assess Pulmonary Absorption and Disposition of Inhaled Therapeutics for Systemic Delivery. *Adv. Drug Deliv. Rev.* **2006**, *58* (9–10), 1030–1060. <https://doi.org/10.1016/j.addr.2006.07.012>.
- (6) Meenach, S. A.; Kim, Y. J.; Kauffman, K. J.; Kanthamneni, N.; Bachelder, E. M.; Ainslie, K. M. Synthesis, Optimization, and Characterization of Camptothecin-Loaded Acetalated Dextran Porous Microparticles for Pulmonary Delivery. *Mol. Pharm.* **2012**, *9* (2), 290–298. <https://doi.org/10.1021/mp2003785>.
- (7) Gradon, L.; Sosnowski, T. R. Formation of Particles for Dry Powder Inhalers. *Adv. Powder Technol.* **2014**, *25* (1), 43–55. <https://doi.org/10.1016/j.apt.2013.09.012>.
- (8) Timsina, M. P.; Martin, G. P.; Marriott, C.; Ganderton, D.; Yianneskis, M. Drug Delivery to the Respiratory Tract Using Dry Powder Inhalers. *Int. J. Pharm.* **1994**, *101* (1–2), 1–13. [https://doi.org/10.1016/0378-5173\(94\)90070-1](https://doi.org/10.1016/0378-5173(94)90070-1).
- (9) Rawal, T.; Parmar, R.; Tyagi, R. K.; Butani, S. Rifampicin Loaded Chitosan Nanoparticle Dry Powder Presents: An Improved Therapeutic Approach for Alveolar Tuberculosis. *Colloids Surfaces B Biointerfaces* **2017**, *154*, 321–330. <https://doi.org/10.1016/j.colsurfb.2017.03.044>.
- (10) Chow, M. Y. T.; Qiu, Y.; Lo, F. F. K.; Lin, H. H. S.; Chan, H. K.; Kwok, P. C. L.; Lam, J. K. W. Inhaled Powder Formulation of Naked siRNA Using Spray Drying Technology with L-Leucine as Dispersion Enhancer. *Int. J. Pharm.* **2017**, *530* (1–2), 40–52. <https://doi.org/10.1016/j.ijpharm.2017.07.013>.
- (11) Kadota, K.; Yanagawa, Y.; Tachikawa, T.; Deki, Y.; Uchiyama, H.; Shirakawa, Y.; Tozuka, Y. Development of Porous Particles Using Dextran as an Excipient for Enhanced Deep Lung Delivery of Rifampicin. *Int. J. Pharm.* **2019**, *555*, 280–290. <https://doi.org/10.1016/j.ijpharm.2018.11.055>.
- (12) Wu, L.; Miao, X.; Shan, Z.; Huang, Y.; Li, L.; Pan, X.; Yao, Q.; Li, G.; Wu, C. Studies on the Spray Dried Lactose as Carrier for Dry Powder Inhalation. *Asian J. Pharm. Sci.* **2014**, *9* (6), 336–341. <https://doi.org/10.1016/j.ajps.2014.07.006>.
- (13) Lohrmann, M.; Kappl, M.; Butt, H. J.; Urbanetz, N. A.; Lippold, B. C. Adhesion Forces in Interactive Mixtures for Dry Powder Inhalers - Evaluation of a New Measuring Method. *Eur. J. Pharm. Biopharm.* **2007**, *67* (2), 579–586. <https://doi.org/10.1016/j.ejpb.2007.02.011>.
- (14) Healy, A. M.; Amaro, M. I.; Paluch, K. J.; Tajber, L. Dry Powders for Oral Inhalation Free of Lactose Carrier

Particles. *Adv. Drug Deliv. Rev.* **2014**, *75*, 32–52. <https://doi.org/10.1016/j.addr.2014.04.005>.

- (15) Hu, J.; Dong, Y.; Kiong, W.; Pastorin, G. Preparation of Drug Nanocrystals Embedded in Mannitol Microcrystals via Liquid Antisolvent Precipitation Followed by Immediate (on-Line) Spray Drying. *Adv. Powder Technol.* **2018**, *29* (4), 957–963. <https://doi.org/10.1016/j.appt.2018.01.013>.
- (16) Kaialy, W. A Review of Factors Affecting Electrostatic Charging of Pharmaceuticals and Adhesive Mixtures for Inhalation. *Int. J. Pharm.* **2016**, *503* (1–2), 262–276. <https://doi.org/10.1016/j.ijpharm.2016.01.076>.
- (17) Mangal, S.; Xu, R.; Park, H.; Zemlyanov, D.; Shetty, N.; Lin, Y. W.; Morton, D.; Chan, H. K.; Li, J.; Zhou, Q. T. Understanding the Impacts of Surface Compositions on the In-Vitro Dissolution and Aerosolization of Co-Spray-Dried Composite Powder Formulations for Inhalation. *Pharm. Res.* **2019**, *36* (1). <https://doi.org/10.1007/s11095-018-2527-x>.
- (18) Shekunov, B. Y.; Chattopadhyay, P.; Tong, H. H. Y.; Chow, A. H. L. Particle Size Analysis in Pharmaceutics: Principles, Methods and Applications. *Pharm. Res.* **2007**, *24* (2), 203–227. <https://doi.org/10.1007/s11095-006-9146-7>.
- (19) Finlay, W. H.; Stapleton, K. W.; Zuberbuhler, P. Fine Particle Fraction as a Measure of Mass Depositing in the Lung during Inhalation of Nearly Isotonic Nebulized Aerosols. *J. Aerosol Sci.* **1997**, *28* (7), 1301–1309. [https://doi.org/10.1016/S0021-8502\(97\)00017-7](https://doi.org/10.1016/S0021-8502(97)00017-7).
- (20) Hickey, A. J.; Martonen, T. B.; Yang, Y. Theoretical Relationship of Lung Deposition to the Fine Particle Fraction of Inhalation Aerosols. *Pharm. Acta Helv.* **1996**, *71* (3), 185–190. [https://doi.org/10.1016/0031-6865\(96\)00014-3](https://doi.org/10.1016/0031-6865(96)00014-3).
- (21) Jetzer, M. W.; Morrical, B. D.; Schneider, M.; Edge, S.; Imanidis, G. Probing the Particulate Microstructure of the Aerodynamic Particle Size Distribution of Dry Powder Inhaler Combination Products. *Int. J. Pharm.* **2018**, *538* (1–2), 30–39. <https://doi.org/10.1016/j.ijpharm.2017.12.046>.
- (22) Otake, H.; Okuda, T.; Okamoto, H. Development of Spray-Freeze-Dried Powders for Inhalation with High Inhalation Performance and Antihygroscopic Property. *Chem. Pharm. Bull.* **2016**, *64* (3), 239–245. <https://doi.org/10.1248/cpb.c15-00824>.
- (23) Sosnik, A.; Seremeta, K. P. Advantages and Challenges of the Spray-Drying Technology for the Production of Pure Drug Particles and Drug-Loaded Polymeric Carriers. *Adv. Colloid Interface Sci.* **2015**, *223*, 40–54. <https://doi.org/10.1016/j.cis.2015.05.003>.
- (24) Chvatal, A.; Ambrus, R.; Party, P.; Katona, G.; Jójárt-Laczko, O.; Szabó-Révész, P.; Fattal, E.; Tsapis, N. Formulation and Comparison of Spray Dried Non-Porous and Large Porous Particles Containing Meloxicam for Pulmonary Drug Delivery. *Int. J. Pharm.* **2019**, *559* (August 2018), 68–75. <https://doi.org/10.1016/j.ijpharm.2019.01.034>.
- (25) Amaro, M. I.; Tewes, F.; Gobbo, O.; Tajber, L.; Corrigan, O. I.; Ehrhardt, C.; Healy, A. M. Formulation, Stability and Pharmacokinetics of Sugar-Based Salmon Calcitonin-Loaded Nanoporous/Nanoparticulate Microparticles (NPMPs) for Inhalation. *Int. J. Pharm.* **2015**, *483* (1–2), 6–18. <https://doi.org/10.1016/j.ijpharm.2015.02.003>.
- (26) Ogi, T.; Nandiyanto, A. B. D.; Okuyama, K. Nanostructuring Strategies in Functional Fine-Particle Synthesis towards Resource and Energy Saving Applications. *Adv. Powder Technol.* **2014**, *25* (1), 3–17. <https://doi.org/10.1016/j.appt.2013.11.005>.

- (27) Parumasivam, T.; Chang, R. Y. K.; Abdelghany, S.; Ye, T. T.; Britton, W. J.; Chan, H. K. Dry Powder Inhalable Formulations for Anti-Tubercular Therapy. *Adv. Drug Deliv. Rev.* **2016**, *102*, 83–101. <https://doi.org/10.1016/j.addr.2016.05.011>.
- (28) Momin, M. A. M.; Tucker, I. G.; Das, S. C. High Dose Dry Powder Inhalers to Overcome the Challenges of Tuberculosis Treatment. *Int. J. Pharm.* **2018**, *550* (1–2), 398–417. <https://doi.org/10.1016/j.ijpharm.2018.08.061>.
- (29) Buttini, F.; Rozou, S.; Rossi, A.; Zoumpliou, V.; Rekkas, D. M. The Application of Quality by Design Framework in the Pharmaceutical Development of Dry Powder Inhalers. *Eur. J. Pharm. Sci.* **2018**, *113* (June 2017), 64–76. <https://doi.org/10.1016/j.ejps.2017.10.042>.
- (30) Higuchi, T. Mechanism of Sustained-action Medication. Theoretical Analysis of Rate of Release of Solid Drugs Dispersed in Solid Matrices. *J. Pharm. Sci.* **1963**, *52* (12), 1145–1149. <https://doi.org/10.1002/jps.2600521210>.
- (31) Lee, H. J.; Lee, H. G.; Kwon, Y. Bin; Kim, J. Y.; Rhee, Y. S.; Chon, J.; Park, E. S.; Kim, D. W.; Park, C. W. The Role of Lactose Carrier on the Powder Behavior and Aerodynamic Performance of Bosentan Microparticles for Dry Powder Inhalation. *Eur. J. Pharm. Sci.* **2018**, *117* (March), 279–289. <https://doi.org/10.1016/j.ejps.2018.03.004>.
- (32) Roos, Y. Melting and Glass Transitions of Low Molecular Weight Carbohydrates. *Carbohydr. Res.* **1993**, *238*, 39–48.
- (33) Zhang, X.; Yue, X.; Cui, Y.; Zhao, Z.; Huang, Y.; Cai, S.; Wang, G.; Wang, W.; Hugh, S.; Pan, X.; Wu, C.; Tan, W. A Systematic Safety Evaluation of Nanoporous Mannitol Material as a Dry-Powder Inhalation Carrier System. *J. Pharm. Sci.* **2020**, *109* (5), 1692–1702. <https://doi.org/10.1016/j.xphs.2020.01.017>.
- (34) Torge, A.; Grützmacher, P.; Mücklich, F.; Schneider, M. The Influence of Mannitol on Morphology and Disintegration of Spray-Dried Nano-Embedded Microparticles. *Eur. J. Pharm. Sci.* **2017**, *104* (April), 171–179. <https://doi.org/10.1016/j.ejps.2017.04.003>.
- (35) Mönckedieck, M.; Kamplade, J.; Fakner, P.; Urbanetz, N. A.; Walzel, P.; Steckel, H.; Scherließ, R. Dry Powder Inhaler Performance of Spray Dried Mannitol with Tailored Surface Morphologies as Carrier and Salbutamol Sulphate. *Int. J. Pharm.* **2017**, *524* (1–2), 351–363. <https://doi.org/10.1016/j.ijpharm.2017.03.055>.
- (36) Mosaiab, T.; Farr, D. C.; Kiefel, M. J.; Houston, T. A. Carbohydrate-Based Nanocarriers and Their Application to Target Macrophages and Deliver Antimicrobial Agents. *Adv. Drug Deliv. Rev.* **2019**, *151–152*, 94–129. <https://doi.org/10.1016/j.addr.2019.09.002>.
- (37) Valente, S. A.; Silva, L. M.; Lopes, G. R.; Sarmiento, B.; Coimbra, M. A.; Passos, C. P. Polysaccharide-Based Formulations as Potential Carriers for Pulmonary Delivery – A Review of Their Properties and Fates. *Carbohydr. Polym.* **2022**, *277* (August 2021), 118784. <https://doi.org/10.1016/j.carbpol.2021.118784>.
- (38) Blanco, D.; Alonso, M. J. Protein Encapsulation and Release from Poly(Lactide-Co-Glycolide) Microspheres: Effect of the Protein and Polymer Properties and of the Co- Encapsulation of Surfactants. *Eur. J. Pharm. Biopharm.* **1998**, *45* (3), 285–294. [https://doi.org/10.1016/S0939-6411\(98\)00011-3](https://doi.org/10.1016/S0939-6411(98)00011-3).
- (39) Péan, J. M.; Venier-Julienne, M. C.; Boury, F.; Menei, P.; Denizot, B.; Benoit, J. P. NGF Release from Poly(D,L-Lactide-Co-Glycolide) Microspheres. Effect of Some Formulation Parameters on Encapsulated NGF Stability. *J. Control. Release* **1998**, *56* (1–3), 175–187. [https://doi.org/10.1016/S0168-3659\(98\)00086-8](https://doi.org/10.1016/S0168-3659(98)00086-8).

- (40) Chang, Y. X.; Yang, J. J.; Pan, R. Le; Chang, Q.; Liao, Y. H. Anti-Hygroscopic Effect of Leucine on Spray-Dried Herbal Extract Powders. *Powder Technol.* **2014**, *266*, 388–395. <https://doi.org/10.1016/j.powtec.2014.06.058>.
- (41) Raula, J.; Kurkela, J. A.; Brown, D. P.; Kauppinen, E. I. Study of the Dispersion Behaviour of L-Leucine Containing Microparticles Synthesized with an Aerosol Flow Reactor Method. *Powder Technol.* **2007**, *177* (3), 125–132. <https://doi.org/10.1016/j.powtec.2007.03.016>.
- (42) Molina, C.; Kaialy, W.; Nokhodchi, A. The Crucial Role of Leucine Concentration on Spray Dried Mannitol-Leucine as a Single Carrier to Enhance the Aerosolization Performance of Albuterol Sulfate. *J. Drug Deliv. Sci. Technol.* **2019**, *49* (September 2018), 97–106. <https://doi.org/10.1016/j.jddst.2018.11.007>.
- (43) Cuvelier, B.; Eloy, P.; Loira-Pastoriza, C.; Ucakar, B.; Sanogo, A. A.; Dupont-Gillain, C.; Vanbever, R. Minimal Amounts of Dipalmitoylphosphatidylcholine Improve Aerosol Performance of Spray-Dried Temocillin Powders for Inhalation. *Int. J. Pharm.* **2015**, *495* (2), 981–990. <https://doi.org/10.1016/j.ijpharm.2015.10.019>.
- (44) Gomez, A. I.; Acosta, M. F.; Muralidharan, P.; Yuan, J. X. J.; Black, S. M.; Hayes, D.; Mansour, H. M. Advanced Spray Dried Proliposomes of Amphotericin B Lung Surfactant-Mimic Phospholipid Microparticles/Nanoparticles as Dry Powder Inhalers for Targeted Pulmonary Drug Delivery. *Pulm. Pharmacol. Ther.* **2020**, *64* (October), 101975. <https://doi.org/10.1016/j.pupt.2020.101975>.
- (45) Kadota, K.; Senda, A.; Ito, T.; Tozuka, Y. Feasibility of Highly Branched Cyclic Dextrin as an Excipient Matrix in Dry Powder Inhalers. *Eur. J. Pharm. Sci.* **2015**, *79*, 79–86. <https://doi.org/10.1016/j.ejps.2015.09.006>.
- (46) Kadota, K.; Nishimura, T.; Hotta, D.; Tozuka, Y. Preparation of Composite Particles of Hydrophilic or Hydrophobic Drugs with Highly Branched Cyclic Dextrin via Spray Drying for Dry Powder Inhalers. *Powder Technol.* **2015**, *283*, 16–23. <https://doi.org/10.1016/j.powtec.2015.05.014>.
- (47) Kadota, K.; Senda, A.; Tagishi, H.; Ayorinde, J. O.; Tozuka, Y. Evaluation of Highly Branched Cyclic Dextrin in Inhalable Particles of Combined Antibiotics for the Pulmonary Delivery of Anti-Tuberculosis Drugs. *Int. J. Pharm.* **2017**, *517* (1–2), 8–18. <https://doi.org/10.1016/j.ijpharm.2016.11.060>.
- (48) Wang, S.; Farnood, R.; Yan, N. Corn-Derived Dendrimer-like Carbohydrate Phytoglycogen Nanoparticles as Selective Fluorescent Sensor for Silver Ions. *Carbohydr. Polym.* **2019**, *223* (January), 115095. <https://doi.org/10.1016/j.carbpol.2019.115095>.
- (49) Nickels, J. D.; Atkinson, J.; Papp-Szabo, E.; Stanley, C.; Diallo, S. O.; Perticaroli, S.; Baylis, B.; Mahon, P.; Ehlers, G.; Katsaras, J.; Dutcher, J. R. Structure and Hydration of Highly-Branched, Monodisperse Phytoglycogen Nanoparticles. *Biomacromolecules* **2016**, *17* (3), 735–743. <https://doi.org/10.1021/acs.biomac.5b01393>.
- (50) Scheffler, S. L.; Huang, L.; Bi, L.; Yao, Y. In Vitro Digestibility and Emulsification Properties of Phytoglycogen Octenyl Succinate. *J. Agric. Food Chem.* **2010**, *58* (8), 5140–5146. <https://doi.org/10.1021/jf904378e>.
- (51) du Toit, L. C.; Pillay, V.; Danckwerts, M. P. Tuberculosis Chemotherapy: Current Drug Delivery Approaches. *Respir. Res.* **2006**, *7*. <https://doi.org/10.1186/1465-9921-7-118>.
- (52) Prota, L.; Santoro, A.; Bifulco, M.; Aquino, R. P.; Mencherini, T.; Russo, P. Leucine Enhances Aerosol Performance of Naringin Dry Powder and Its Activity on Cystic Fibrosis Airway Epithelial Cells. *Int. J. Pharm.* **2011**, *412* (1–2), 8–19. <https://doi.org/10.1016/j.ijpharm.2011.03.055>.
- (53) Vehring, R. Pharmaceutical Particle Engineering via Spray Drying. *Pharm. Res.* **2008**, *25* (5), 999–1022.

<https://doi.org/10.1007/s11095-007-9475-1>.

- (54) Zeng, X. M.; Martin, G. P.; Marriott, C.; Pritchard, J. Lactose as a Carrier in Dry Powder Formulations: The Influence of Surface Characteristics on Drug Delivery. *J. Pharm. Sci.* **2001**, *90* (9), 1424–1434. <https://doi.org/10.1002/jps.1094>.
- (55) Karhu, M.; Kuikka, J.; Kauppinen, T.; Bergström, K.; Vidgren, M. Pulmonary Deposition of Lactose Carriers Used in Inhalation Powders. *Int. J. Pharm.* **2000**, *196* (1), 95–103. [https://doi.org/10.1016/S0378-5173\(99\)00450-0](https://doi.org/10.1016/S0378-5173(99)00450-0).
- (56) He, Y.; Liang, Y.; Han, R.; Lu, W. L.; Mak, J. C. W.; Zheng, Y. Rational Particle Design to Overcome Pulmonary Barriers for Obstructive Lung Diseases Therapy. *J. Control. Release* **2019**, *314* (August), 48–61. <https://doi.org/10.1016/j.jconrel.2019.10.035>.
- (57) Hickey, A. J. Emerging Trends in Inhaled Drug Delivery. *Adv. Drug Deliv. Rev.* **2020**, *157*, 63–70. <https://doi.org/10.1016/j.addr.2020.07.006>.
- (58) Gradon, L.; Sosnowski, T. R. Formation of Particles for Dry Powder Inhalers. *Adv. Powder Technol.* **2014**, *25* (1), 43–55. <https://doi.org/10.1016/j.apt.2013.09.012>.
- (59) Edwards, D. A.; Hanes, J.; Caponetti, G.; Hrkach, J.; Ben-Jebria, A.; Eskew, M. Lou; Mintzes, J.; Deaver, D.; Lotan, N.; Langer, R. Large Porous Particles for Pulmonary Drug Delivery. *Science* (80-.). **1997**, *276* (5320), 1868–1871. <https://doi.org/10.1126/science.276.5320.1868>.
- (60) Patel, B.; Gupta, V.; Ahsan, F. PEG-PLGA Based Large Porous Particles for Pulmonary Delivery of a Highly Soluble Drug, Low Molecular Weight Heparin. *J. Control. Release* **2012**, *162* (2), 310–320. <https://doi.org/10.1016/j.jconrel.2012.07.003>.
- (61) Lintingre, E.; Lequeux, F.; Talini, L.; Tsapis, N. Control of Particle Morphology in the Spray Drying of Colloidal Suspensions. *Soft Matter* **2016**, *12* (36), 7435–7444. <https://doi.org/10.1039/c6sm01314g>.
- (62) Archer, J.; Walker, J.; Gregson, F. K. A.; Hardy, D. A.; Reid, J. P. Drying Kinetics and Particle Formation from Dilute Colloidal Suspensions in Aerosol Droplets. *Langmuir* **2020**. <https://doi.org/10.1021/acs.langmuir.0c01830>.
- (63) Nandiyanto, A. B. D.; Okuyama, K. Progress in Developing Spray-Drying Methods for the Production of Controlled Morphology Particles: From the Nanometer to Submicrometer Size Ranges. *Adv. Powder Technol.* **2011**, *22* (1), 1–19. <https://doi.org/10.1016/j.apt.2010.09.011>.
- (64) Wang, W. N.; Purwanto, A.; Lenggoro, I. W.; Okuyama, K.; Chang, H.; Jang, H. D. Investigation on the Correlations between Droplet and Particle Size Distribution in Ultrasonic Spray Pyrolysis. *Ind. Eng. Chem. Res.* **2008**, *47* (5), 1650–1659. <https://doi.org/10.1021/ie070821d>.
- (65) Hewitt, A. J. Droplet Size Spectra Produced by Air-Assisted Atomizers. *J. Aerosol Sci.* **1993**, *24* (2), 155–162.
- (66) De Boer, A. H.; Dickhoff, B. H. J.; Hagedoorn, P.; Gjaltema, D.; Goede, J.; Lambregts, D.; Frijlink, H. W. A Critical Evaluation of the Relevant Parameters for Drug Redispersion from Adhesive Mixtures during Inhalation. *Int. J. Pharm.* **2005**, *294* (1–2), 173–184. <https://doi.org/10.1016/j.ijpharm.2005.01.035>.
- (67) Iida, K.; Hayakawa, Y.; Okamoto, H.; Danjo, K.; Leuenberger, H. Evaluation of Flow Properties of Dry Powder Inhalation of Salbutamol Sulfate with Lactose Carrier. *Chem. Pharm. Bull.* **2001**, *49* (10), 1326–1330. <https://doi.org/10.1248/cpb.49.1326>.
- (68) Hwang, S. M.; Kim, D. D.; Chung, S. J.; Shim, C. K. Delivery of Ofloxacin to the Lung and Alveolar Macrophages

via Hyaluronan Microspheres for the Treatment of Tuberculosis. *J. Control. Release* **2008**, *129* (2), 100–106. <https://doi.org/10.1016/j.jconrel.2008.04.009>.

- (69) Vadakkan, M. V.; Annapoorna, K.; Sivakumar, K. C.; Mundayoor, S.; Kumar, G. S. V. Dry Powder Cationic Lipopolymeric Nanomicelle Inhalation for Targeted Delivery of Antitubercular Drug to Alveolar Macrophage. *Int. J. Nanomedicine* **2013**, *8*, 2871–2885. <https://doi.org/10.2147/IJN.S47456>.
- (70) Diab, R.; Brillault, J.; Bardy, A.; Gontijo, A. V. L.; Olivier, J. C. Formulation and in Vitro Characterization of Inhalable Polyvinyl Alcohol-Free Rifampicin-Loaded PLGA Microspheres Prepared with Sucrose Palmitate as Stabilizer: Efficiency for Ex Vivo Alveolar Macrophage Targeting. *Int. J. Pharm.* **2012**, *436* (1–2), 833–839. <https://doi.org/10.1016/j.ijpharm.2012.07.036>.
- (71) Weiss, G.; Schaible, U. E. Macrophage Defense Mechanisms against Intracellular Bacteria. *Immunol. Rev.* **2015**, *264* (1), 182–203. <https://doi.org/10.1111/imr.12266>.
- (72) Liu, Y. C.; Zou, X. B.; Chai, Y. F.; Yao, Y. M. Macrophage Polarization in Inflammatory Diseases. *Int. J. Biol. Sci.* **2014**, *10* (5), 520–529. <https://doi.org/10.7150/ijbs.8879>.
- (73) Yin, M.; Zhang, Y.; Li, H. Advances in Research on Immunoregulation of Macrophages by Plant Polysaccharides. *Front. Immunol.* **2019**, *10* (FEB). <https://doi.org/10.3389/fimmu.2019.00145>.
- (74) Kusaka, T.; Nakayama, M.; Nakamura, K.; Ishimiya, M.; Furusawa, E.; Ogasawara, K. Effect of Silica Particle Size on Macrophage Inflammatory Responses. *PLoS One* **2014**, *9* (3), 1–9. <https://doi.org/10.1371/journal.pone.0092634>.
- (75) Wijagkanalan, W.; Kawakami, S.; Takenaga, M.; Igarashi, R.; Yamashita, F.; Hashida, M. Efficient Targeting to Alveolar Macrophages by Intratracheal Administration of Mannosylated Liposomes in Rats. *J. Control. Release* **2008**, *125* (2), 121–130. <https://doi.org/10.1016/j.jconrel.2007.10.011>.
- (76) Gupta, P. K.; Rajan, M. G. R.; Kulkarni, S. Activation of Murine Macrophages by G1-4A, a Polysaccharide from *Tinospora Cordifolia*, in TLR4/MyD88 Dependent Manner. *Int. Immunopharmacol.* **2017**, *50* (March), 168–177. <https://doi.org/10.1016/j.intimp.2017.06.025>.
- (77) Gitsov, I.; Fréchet, J. M. J. Stimuli-Responsive Hybrid Macromolecules: Novel Amphiphilic Star Copolymers with Dendritic Groups at the Periphery. *J. Am. Chem. Soc.* **1996**, *118* (15), 3785–3786. <https://doi.org/10.1021/ja9542348>.
- (78) Esquenet, C.; Buhler, E. Aggregation Behavior in Semidilute Rigid and Semirigid Polysaccharide Solutions. *Macromolecules* **2002**, *35* (9), 3708–3716. <https://doi.org/10.1021/ma012047q>.
- (79) Tsapis, N.; Bennett, D.; Jackson, B.; Weitz, D. A.; Edwards, D. A. Trojan Particles: Large Porous Carriers of Nanoparticles for Drug Delivery. *Proc. Natl. Acad. Sci. U. S. A.* **2002**, *99* (19), 12001–12005. <https://doi.org/10.1073/pnas.182233999>.
- (80) Lin, J. C.; Gentry, J. W. Spray Drying Drop Morphology: Experimental Study. *Aerosol Sci. Technol.* **2003**, *37* (1), 15–32. <https://doi.org/10.1080/02786820300888>.
- (81) Nandiyanto, A. B. D.; Hagura, N.; Iskandar, F.; Okuyama, K. Design of a Highly Ordered and Uniform Porous Structure with Multisized Pores in Film and Particle Forms Using a Template-Driven Self-Assembly Technique. *Acta Mater.* **2010**, *58* (1), 282–289. <https://doi.org/10.1016/j.actamat.2009.09.004>.

- (82) Cheow, W. S.; Li, S.; Hadinoto, K. Spray Drying Formulation of Hollow Spherical Aggregates of Silica Nanoparticles by Experimental Design. *Chem. Eng. Res. Des.* **2010**, *88* (5–6), 673–685. <https://doi.org/10.1016/j.cherd.2009.11.012>.
- (83) Borgström, L.; Olsson, B.; Thorsson, L. Degree of Throat Deposition Can Explain the Variability in Lung Deposition of Inhaled Drugs. *J. Aerosol Med. Depos. Clear. Eff. Lung* **2006**, *19* (4), 473–483. <https://doi.org/10.1089/jam.2006.19.473>.
- (84) Cal, K.; Sollohub, K. Spray Drying Technique. I: Hardware and Process Parameters. *J. Pharm. Sci.* **2010**, *99* (5), 575–586. <https://doi.org/10.1002/jps>.
- (85) Muzaffar, K.; Kumar, P. Parameter Optimization for Spray Drying of Tamarind Pulp Using Response Surface Methodology. *Powder Technol.* **2015**, *279*, 179–184. <https://doi.org/10.1016/j.powtec.2015.04.010>.
- (86) Wanning, S.; Süverkrüp, R.; Lamprecht, A. Pharmaceutical Spray Freeze Drying. *Int. J. Pharm.* **2015**, *488* (1–2), 136–153. <https://doi.org/10.1016/j.ijpharm.2015.04.053>.
- (87) Wang, Z.; Meenach, S. A. Optimization of Acetalated Dextran–Based Nanocomposite Microparticles for Deep Lung Delivery of Therapeutics via Spray-Drying. *J. Pharm. Sci.* **2017**, *106* (12), 3539–3547. <https://doi.org/10.1016/j.xphs.2017.07.022>.
- (88) Kanojia, G.; Willems, G. J.; Frijlink, H. W.; Kersten, G. F. A.; Soema, P. C.; Amorij, J. P. A Design of Experiment Approach to Predict Product and Process Parameters for a Spray Dried Influenza Vaccine. *Int. J. Pharm.* **2016**, *511* (2), 1098–1111. <https://doi.org/10.1016/j.ijpharm.2016.08.022>.
- (89) Li, H. Y.; Birchall, J. Chitosan-Modified Dry Powder Formulations for Pulmonary Gene Delivery. *Pharm. Res.* **2006**, *23* (5), 941–950. <https://doi.org/10.1007/s11095-006-0027-x>.
- (90) Gliński, J.; Chavepeyer, G.; Platten, J. K. Surface Properties of Aqueous Solutions of L-Leucine. *Biophys. Chem.* **2000**, *84* (2), 99–103. [https://doi.org/10.1016/S0301-4622\(99\)00150-7](https://doi.org/10.1016/S0301-4622(99)00150-7).
- (91) Lu, W.; Rades, T.; Rantanen, J.; Chan, H. K.; Yang, M. Amino Acids as Stabilizers for Spray-Dried Simvastatin Powder for Inhalation. *Int. J. Pharm.* **2019**, *572* (August), 118724. <https://doi.org/10.1016/j.ijpharm.2019.118724>.
- (92) Gallo, L.; Ramírez-rigo, M. V.; Bucalá, V. Development of Porous Spray-Dried Inhalable Particles Using an Organic Solvent-Free Technique. *Powder Technol.* **2019**, *342*, 642–652. <https://doi.org/10.1016/j.powtec.2018.10.041>.
- (93) Nair, A.; Khunt, D.; Misra, M. Application of Quality by Design for Optimization of Spray Drying Process Used in Drying of Risperidone Nanosuspension. *Powder Technol.* **2019**, *342*, 156–165. <https://doi.org/10.1016/j.powtec.2018.09.096>.
- (94) Saha, D.; Nanda, S. K.; Yadav, D. N. Optimization of Spray Drying Process Parameters for Production of Groundnut Milk Powder. *Powder Technol.* **2019**, *355*, 417–424. <https://doi.org/10.1016/j.powtec.2019.07.066>.
- (95) Gu, B.; Linehan, B.; Tseng, Y. C. Optimization of the Büchi B-90 Spray Drying Process Using Central Composite Design for Preparation of Solid Dispersions. *Int. J. Pharm.* **2015**, *491* (1–2), 208–217. <https://doi.org/10.1016/j.ijpharm.2015.06.006>.
- (96) Kugler, S.; Nagy, A.; Kerekes, A.; Veres, M.; Rigó, I.; Czitrovsky, A. Determination of Emitted Particle Characteristics and Upper Airway Deposition of Symbicort® Turbuhaler® Dry Powder Inhaler. *J. Drug Deliv. Sci.*

Technol. **2019**, *54* (May), 101229. <https://doi.org/10.1016/j.jddst.2019.101229>.

- (97) Abadelah, M.; Hazim, F.; Chrystyn, H.; Bagherisadeghi, G.; Rahmoune, H.; Larhrib, H. Effect of Maximum Inhalation Flow and Inhaled Volume on Formoterol Drug Deposition In-Vitro from an Easyhaler® Dry Powder Inhaler. *Eur. J. Pharm. Sci.* **2017**, *104* (March), 180–187. <https://doi.org/10.1016/j.ejps.2017.03.035>.
- (98) De Boer, A. H.; Gjaltema, D.; Hagedoorn, P.; Frijlink, H. W. Can “extrafine” Dry Powder Aerosols Improve Lung Deposition? *Eur. J. Pharm. Biopharm.* **2015**, *96*, 143–151. <https://doi.org/10.1016/j.ejpb.2015.07.016>.
- (99) Al Zaitone, B.; Al-zahrani, A.; Al-shahrani, S.; Lamprecht, A. Drying of a Single Droplet of Dextrin : Drying Kinetics Modeling and Particle Formation. *Int. J. Pharm.* **2020**, *574* (November 2019), 118888. <https://doi.org/10.1016/j.ijpharm.2019.118888>.
- (100) Maury, M.; Murphy, K.; Kumar, S.; Shi, L.; Lee, G. Effects of Process Variables on the Powder Yield of Spray-Dried Trehalose on a Laboratory Spray-Dryer. *Eur. J. Pharm. Biopharm.* **2005**, *59* (3), 565–573. <https://doi.org/10.1016/j.ejpb.2004.10.002>.
- (101) Focaroli, S.; Mah, P. T.; Hastedt, J. E.; Gitlin, I.; Oscarson, S.; Fahy, J. V.; Healy, A. M. A Design of Experiment (DoE) Approach to Optimise Spray Drying Process Conditions for the Production of Trehalose/Leucine Formulations with Application in Pulmonary Delivery. *Int. J. Pharm.* **2019**, *562* (November 2018), 228–240. <https://doi.org/10.1016/j.ijpharm.2019.03.004>.
- (102) Jaskulski, M.; Wawrzyniak, P.; Zbiciński, I. CFD Simulations of Droplet and Particle Agglomeration in an Industrial Counter-Current Spray Dryer. *Adv. Powder Technol.* **2018**, *29* (7), 1724–1733. <https://doi.org/10.1016/j.appt.2018.04.007>.
- (103) Qian, J.; Law, C. K. Regimes of Coalescence and Separation in Droplet Collision. *J. Fluid Mech.* **1997**, *331*, 59–80. <https://doi.org/10.1017/S0022112096003722>.
- (104) Orme, M. Experiments on Droplet Collisions, Bounce, Coalescence and Disruption. *Prog. Energy Combust. Sci.* **1997**, *23* (1), 65–79. [https://doi.org/10.1016/s0360-1285\(97\)00005-1](https://doi.org/10.1016/s0360-1285(97)00005-1).
- (105) Pham, D. D.; Fattal, E.; Ghermani, N. E.; Guiblin, N.; Tsapis, N. Formulation of Pyrazinamide-Loaded Large Porous Particles for the Pulmonary Route: Avoiding Crystal Growth Using Excipients. *Int. J. Pharm.* **2013**, *454* (2), 668–677. <https://doi.org/10.1016/j.ijpharm.2013.04.016>.
- (106) Son, Y. J.; Worth Longest, P.; Hindle, M. Aerosolization Characteristics of Dry Powder Inhaler Formulations for the Excipient Enhanced Growth (EEG) Application: Effect of Spray Drying Process Conditions on Aerosol Performance. *Int. J. Pharm.* **2013**, *443* (1–2), 137–145. <https://doi.org/10.1016/j.ijpharm.2013.01.003>.
- (107) Pornputtapitak, W.; El-gendy, N.; Berkland, C. Nanocluster Budesonide Formulations Enhance Drug Delivery through Endotracheal Tubes. *J. Pharm. Sci.* **2012**, *101* (3), 1063–1072. <https://doi.org/10.1002/jps.22818>.
- (108) Tse, J. Y.; Kadota, K.; Hirata, Y.; Taniguchi, M.; Uchiyama, H.; Tozuka, Y. Characterization of Matrix Embedded Formulations for Combination Spray-Dried Particles Comprising Pyrazinamide and Rifampicin. *J. Drug Deliv. Sci. Technol.* **2018**, *48*, 137–144. <https://doi.org/10.1016/j.jddst.2018.09.013>.

Published articles

1. Tse, J. Y.; Kadota, K.; Imakubo, T.; Uchiyama, H.; Tozuka, Y. Enhancement of the Extra-Fine Particle Fraction of Levofloxacin Embedded in Excipient Matrix Formulations for Dry Powder Inhaler Using Response Surface Methodology. *Eur. J. Pharm. Sci.* **2021**, *156*, 105600. <https://doi.org/10.1016/j.ejps.2020.105600>.
2. Tse, J. Y.; Koike, A.; Kadota, K.; Uchiyama, H.; Fujimori, K.; Tozuka, Y. Porous Particles and Novel Carrier Particles with Enhanced Penetration for Efficient Pulmonary Delivery of Antitubercular Drugs. *Eur. J. Pharm. Biopharm.* **2021**, *167* (April), 116–126. <https://doi.org/10.1016/j.ejpb.2021.07.017>.

Relevant articles

1. Tse, J. Y.; Kadota, K.; Hirata, Y.; Taniguchi, M.; Uchiyama, H.; Tozuka, Y. Characterization of Matrix Embedded Formulations for Combination Spray-Dried Particles Comprising Pyrazinamide and Rifampicin. *J. Drug Deliv. Sci. Technol.* **2018**, *48*, 137–144. <https://doi.org/10.1016/j.jddst.2018.09.013>.
2. Tse, J. Y.; Kadota, K.; Yang, Z.; Uchiyama, H.; Tozuka, Y. Investigation the molecular state of 4-aminosalicylic acid in matrix formulations for dry powder inhalers using solid-state fluorescence spectroscopy of 4-dimethylaminobenzonitrile. *Adv. Powder Technol.* **2019**, *30*, 2422–2429. <https://doi.org/10.1016/j.apt.2019.07.027>
3. Kadota, K.; Sosnowski, T. R.; Tobita, S.; Tachibana, I.; Tse, J. Y.; Uchiyama, H.; Tozuka, Y. A Particle Technology Approach toward Designing Dry-Powder Inhaler Formulations for Personalized Medicine in Respiratory Diseases. *Adv. Powder Technol.* **2020**, *31* (1), 219–226. <https://doi.org/10.1016/j.apt.2019.10.013>.